Experimental Investigation on the Influence of Surface Defects on High-Speed Gear Performance

Undergraduate Honors Thesis

Presented in Partial Fulfillment of the Requirements for Graduation with Honors Research Distinction in the Department of Mechanical Engineering at The Ohio State University

By

Günther Shepard Beall

Undergraduate Honors Program in Mechanical Engineering

The Ohio State University

2020

Thesis Committee

Dr. Ahmet Kahraman, Advisor

Dr. Michael Handschuh, Co-Advisor

Dr. David Talbot

ABSTRACT

Gear tooth surfaces may contain undesirable defects for various reasons. One class of defects, surface scratches, are primarily related to manufacturing and assembly errors. The durability consequences of scratches have yet to be investigated. In this study, singular calibrated scratches varying in location and orientation are applied to the tooth surfaces of three otherwise high-quality, aerospace grade spur gears. These gears, along with a baseline undamaged control gear pair, are put through staged scuffing experiments that incrementally increased torque, operating speed, and bulk lubricant temperature at aerospace operating conditions. Gear coordinate measurements are performed initially to verify scratch location and that gear geometries and micro-geometries are within the specifications. Throughout testing, nondestructive metrology techniques involving microscope imaging and probe roughness traces are used at various sites along the scratch to track scratch-induced surface damage and changes in scratch geometry. All three gear pairs with scratched pinions are shown to experience scuffing failures in the early stages of tests in comparison to the scratch-free baseline gear. It is concluded that (i) surface scratches indeed impact the scuffing performance, (ii) the positive material generated during scratching has little influence on scuffing performance, and (iii) that there is no evidence of scratches healing or wearing away during operation.

DEDICATION

This thesis is dedicated to my grandparents William and Janet Beall, and Edward and Kathleen Timerson, whose unconditional love and support have provided me the character and resources needed to turn dreams into reality.

ACKNOWLEDGEMENTS

My sincerest thanks to my advisor, Dr. Ahmet Kahraman for presenting me with this opportunity and for his guidance throughout the project. I would also like to thank Dr. Michael Handschuh for his tireless mentorship on the operation of the test machines, the metrological procedures involved, and the writing of this thesis. Finally, I would like to acknowledge Pratt and Whitney for their funding and support of this project.

VITA

December 21, 1997……..……Born – Columbus, Ohio

2018 – Present……Undergraduate Teaching Assistant, The Ohio State University

2018 – Present…… Undergraduate Research Assistant, The Ohio State University

2020 – Present....……Engineering Intern, CORE Molding Technologies

Field of Study

Major Field: Mechanical Engineering

TABLE OF CONTENTS

LIST OF TABLES

LIST OF FIGURES

NOMENCLATURE

Symbol	Definition
α	scratch positive material height coefficient
β	scratch peak-to-peak distance coefficient
γ	scratch positive material half-width coefficient
H	scratch peak-to-valley height
HPSTC	highest point of single tooth contact
LOA	line of action
LPSTC	lowest point of single tooth contact
R_a	mean roughness amplitude
R_q	root-mean-square roughness amplitude
T	reference pinion torque

CHAPTER 1

INTRODUCTION

1.1 Background and Motivation

Gears used in aerospace applications must endure challenging operating conditions defined by very high speeds and elevated temperatures. Any manufacturing errors at high-speed conditions, regardless of how small they are, must be viewed with great caution to prevent any harmful dynamic consequences. Likewise, minor surface defects that could result in hot spots on the contact surfaces of gears are treated critically.

While every attempt is made to minimize manufacturing errors and defects, there may still be some minor defects that could be tolerated since they might not pose significant negative consequence. This study focuses on an investigation of gear tooth surface defects that are often unintentionally introduced to the gears in aerospace gearboxes. It is intended to provide clues on what level of damage or defect can be tolerated without compromising the performance of the system. If the severity of the defects can be related to the resultant degradation of performance, this would provide significant cost savings, as not every gear with a defect would be scrapped.

The contact and bending fatigue performance of gears is typically not impacted by minor surface defects. However, a surface failure known as scuffing may be very susceptible to surface defects if they are locations where tooth contact take place. Scuffing is an instantaneous adhesion and tearing of two surfaces that come into sliding contact at a sufficiently high pressure and temperature. This leaves the surface plastically deformed. Higher levels of asperity (metal-to-metal) contacts of tooth surfaces are known to enhance the chances of scuffing [1–3]. As such, many aerospace gears are subjected to final surface finishing processes to reduce their surface roughness amplitudes caused by cutting processes such as grinding. A recent study conducted by Handschuh et al. [4,5] indicated that scuffing can occur when the surfaces are smoothened as well. In such cases, they showed that the fluid film temperature and the contact pressure collectively define a scuffing limit. Regardless, the onset of a scuffing failure is usually progressive, starting at locations of highest heat generation. Locations with any surface defects are good candidates for the formation of hot spots that lead to scuffing.

Gear contact surfaces are ideally separated by a very thin layer of lubricant, whose formation is determined by principles of elastohydrodynamic lubrication (EHL). While the length of the contact along the face width of the gear teeth is typically large, width of the contact along the profile direction is rather narrow. Any defect of sizes comparable to the instantaneous contact footprint could cause the EHL conditions to be altered significantly with some adverse results.

While surface defects can be different shapes, occurring at different locations on a tooth surface, a common type is scratches induced by poor handling of the finished gears.

These scratches can be of certain width and depth extending along the width of the tooth or diagonally or radially. Some of these scratches can self-heal during the initial run-in stages of the operation while others might cause catastrophic scuffing failures. A feasibility study on how to quantify the impact of surface scratches on scuffing is the main goal of this study.

1.2 Literature Review

A series of papers by Dowson et al. [6–10] proposed solutions for EHL contact models. These solutions provide fundamental estimations for the contact area and film thickness of EHL contacts. It was theorized that at EHL conditions, rolling velocity and material modulus are proportional to film thickness, while load was inversely proportional.

Scuffing occurs as a result of lubricant failure. A robust, relatively fast EHL model was developed by Li and Kahraman [1]. This model could predict extensive asperity interactions at low speeds on ground contacts. Heat transfer and thermal effects were added to this model by Liou [2]. This model was further refined and used by Li et and Kahraman [3] to propose that asperity interactions increase the contact flash temperature up to a maximum local temperature at which point scuffing initiates. This theory was explored with ball-on-disk experiments having a super-finished ball and radially ground ball. However, this model fails to explain scuffing failures observed on super-finished contacts where asperity interactions are low, as is the case with the gears in this study. Coupling experiments with the model from Ref. [3], Handschuh et al. [5] showed that a pressure-temperature relationship effectively described a set of two-disk tribometer scuffing

experiments. It was postulated that local heating due to fluid shear caused the lubricant to fail, resulting in scuffing failure. The scuffing limit was linked to the local pressure and mid-layer fluid temperature and the contact was more resistive to scuffing at elevated pressures.

In order to replicate harsh aerospace contact conditions, specifically developed test machines were developed and validated by Leque [11]. Further experiments by Olson [12] and Brenneman [13] on these machines showed that decreasing surface roughness and performing run-ins on gears improved surface fatigue life and scuffing resistance. This was also demonstrated by Krantz et al. [14] using two offset 28-tooth spur gears made from 9310 gear steel. Patching et al. [15] observed that scuffing load increased as surface finish was improved on a two-disk tribometer setup.

Dempsey et al. [16,17] developed and validated a Health Usage Monitoring System (HUMS) for helicopter transmissions that measured gearbox vibrations and debris concentration in the oil stream to predict gearbox fatigue failure. It was determined that debris size alone could not distinguish between bearing and gear fatigue and failure. Additionally, gears with known faults were tested to show that HUMS could detect impending failures and replace traditional maintenance inspections. Brennan and Reynolds [18] attempted to use demodulation, a wavelet transform, and analyzing the kurtosis of vibration measurements to detect defects in gear teeth. However, no method provided an obvious, robust indicator of defect presence.

Scratch geometries were simulated by Lubrecht et al. [19] and used in dry contact models of point and line contacts to estimate surface life reduction in the form of surface

fatigue. However, time and computational power limitations resulted in life reduction to be underestimated. Utsave and Li [20] simulated micro-dimples in a thermal EHL model, which predicted increased pressure and asperity interaction at the circumference of these dimples.

An experimental study performed by Lim [21] investigated the generation of radially oriented debris-induced damage on aerospace-grade spur gears. The damaged gears were then run through a series of high-speed high-temperature tests that incrementally increased the torque, speed, and oil temperature to test the gears' scuffing susceptibility. It was observed that debris caused the most damage about points of high sliding in the contact. Additionally, the results showed that by increased damage severity, scuffing performance was diminished.

There is a gap in existing literature regarding how and what size macroscopic surface defects impact the gear performance adversely. The scope of this study will be on the effects of precise, singular scratches applied at predetermined tooth surface locations on the scuffing performance of polished gears running under high-speed aerospace conditions. Ultimately, the goal of this study is to provide guidance on scratches of what severity can be tolerated by the gear contacts.

1.3 Scope and Objectives

This study will focus on the generation and measurement of tightly controlled scratches on otherwise acceptable spur gear specimens throughout scuffing tests. These

scratches were parameterized by size, location, and orientation. The specific objectives of this study are as follows:

- Generate controlled scratches parameterized by size (width and depth), location, and orientation on otherwise acceptable spur gear specimens.
- Develop nondestructive metrological procedures for quantifying scratch geometries and their evolution throughout the operation of a gear.
- Perform high-speed gear scuffing tests to correlate the presence of applied scratches with adverse gear scuffing performance and create guidelines to isolate permissible scratch severity for production gears.

1.4 Thesis Outline

Following the guidance of the specific objectives described above, the work will be described in two main chapters. Chapter 2 details the experimental setup, test methodology, and metrological procedures used to complete this study. Information on gear geometries, test conditions, and defect generation can also be found in this chapter. Chapter 3 provides results from an undamaged control gear pair, as well as results and insights from the three gear pairs tested with intentional scratch damage. Important collected data and the conclusions that have been drawn from them are included in this chapter. Chapter 4 provides a high-level recapitulation of this thesis. Details from all three preceding chapters are covered here.

CHAPTER 2

EXPERIMENTAL TEST METHODOLOGY

2.1 Introduction

Concerns regarding the adverse effects of surface defects and surface irregularities stem from the extreme operating conditions aerospace gearboxes must withstand without failure. Isolating and replicating these conditions reliably in a controlled lab environment is challenging. A high-speed machine set-up [11] developed specifically to emulate aerospace gear conditions that was later employed for other specific investigations [12,13,21] will be used here. High-quality spur gear specimens will be intentionally compromised by applying calibrated scratches that replicate the common form of surface damage observed in practice. The consequences of scratch location and orientation on the scuffing performance of the gears will be investigated.

This chapter introduces the experimental test set-up. The baseline spur gear test specimens are presented. The size, location, and orientation of the applied scratches are described along with the test and inspection procedures governing these experiments.

2.2 Experimental Test Set-up

The most common arrangement for a gear test machine is a four-square back-to-back type, which has several advantages. Figure 2.1 images the experimental setup. The main components of the test machines are schematized in Figure 2.2. These machines are fundamentally equivalent to International Organization of Standardization (ISO) standard gearboxes [22] except they can operate at speeds nearly 5 times greater. In this set-up, two gear boxes are connected via two parallel shafts to create a closed loop. For the remainder of this document, the frontmost gearbox will referred to as the test gearbox, while the rearmost gearbox will be called the reaction gearbox. The benefit of this setup is that when one shaft is clocked relative to the other(s), a static torque develops inside the loop. As a result, the drive motor is only required to provide sufficient torque to overcome the frictional losses associated with driving the gearboxes, while high loads can be applied to the gears through a torque actuator.

Elastomer flex-couplings connect the test and reaction gearboxes between the two long and compliant shafts. This mechanically filters vibrations between the two gearboxes while allowing for machine disassembly. Because representative aerospace conditions are targeted, high-speed and high-temperature oil conditions were considered with these machines. The elaborate jet lubrication systems and hydraulic torque actuation featured on these machines distinguish them from ISO standard machines that are suitable for lower speed automotive applications. As these machines were described in extensively in Refs. [11–13,21], only the germane technical information will be provided here for completeness.

Figure 2.1: Overall view of the high-speed test machines used in this study.

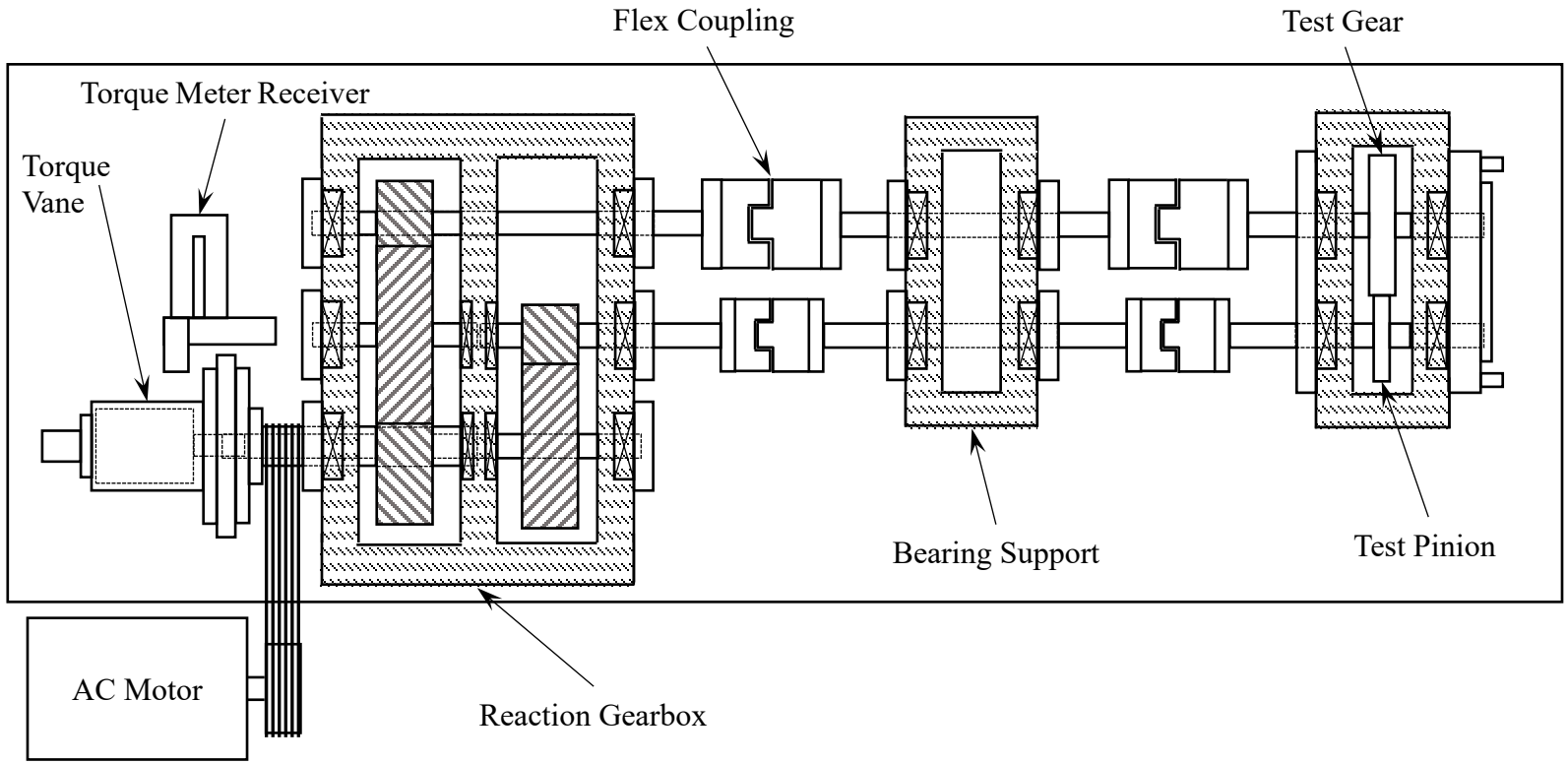

Figure 2.2: Top-view schematic of the high-speed test machine with its main components labeled.

These high-speed machines use separate lubrication systems for the reaction and test gearboxes. This facilitates the use of optimal lubricants and temperatures for the life of the reaction gearbox (i.e. thick, cool hydraulic oil), while allowing test-specific lubricants and temperatures to be used in the test gearbox. The test gearbox lubrication system consists of both heating and cooling loops to control the temperature of the oil and digital flow meters to deliver precise amounts of lubricant to the gear contact.

The reaction gearbox was intentionally overdesigned to prevent any type of gear failure (e.g. bending, contact fatigue and scuffing). As such, it differs from the standard design in several aspects. Referring to Figure 2.2, the reaction gearbox consists of five gears rather than the traditional pair in a standard four-square arrangement. High pinion-shaft speeds necessitated the additional reaction gearbox complexity. Additionally, the torque actuator, torque-meter, and rotary union are cantilevered off the backside of the reaction gearbox, requiring lower rotational speeds. The larger diameter input gear increases the speed to the test gearbox by a factor of 2.18.

In an ISO standard test machine, a split coupling along either the pinion or gear shaft is used to mechanically induce torque within the system by fixing one half of the coupling and clocking the other by hanging weights. This approach is simple in nature and requires no additional equipment or controls. However, changing the torque requires the machine to be stopped, coupling disengaged, and new weights hung. The high-speed machines used in this study were equipped with hydraulic, rotary torque-vane actuators. In this setup, as shown in Figure 2.2, coaxial shafts are rotated relative to each other to induce torque within the loop. Although hydraulics and an accompanying control system are

required, the applied torque can be changed without stopping a high-speed test. The continuously variable operating conditions are useful in mimicking different duty cycle conditions. A 40 HP AC electric motor is attached to the outer torque vane shaft by six V-belts to input rotational velocity to the gear shafts.

The test gearbox contained the experimental 17-tooth pinion and 26-tooth gear pair at the ISO standard center distance of 91.5 mm (3.6 in). The high-speed machines were designed to reach a maximum pinion speed of 13,500 rpm at a pinion torque of 450 Nm (330 ft-lb). This corresponds to a pitch-line velocity slightly larger than 50 m/s (10,000 ft/min). Two in-line heaters were added to the machines to deliver lubricant up to 160°C at a maximum rate of 4 liters/min (about 1 gal/min).

Several measurement devices provided continual feedback and monitoring of important parameters and components. A torque meter measured the applied torque from the hydraulic actuator and used feedback control to maintain the desired conditions. The torque meter was rated to 565 Nm with an accuracy of 0.05% full-scale (i.e. $\pm$ 0.3 Nm). A magnetic pickup was used to measure the rotational speed of the pinion shaft. Thermocouples were used to control the inlet lubricant temperature and assess the health of the bearings contained in each gearbox. Accelerometers were used to record vibration levels, which were used to identify scuffing failures. Flowmeters and needle valves were used to precisely control the amount of lubricant delivered to the gear mesh.

2.3 Gear Specimens

The spur gear pair design used in this study had a 17-26 ratio. The basic design parameters of this gear pair are listed in Table 2.1. The gear pair had certain profile microgeometry modifications to minimize transmission error, a noise metric, under the range of operating conditions. Additionally, lead modifications centered the force carried by the tooth pair.

An image of the nominal gear pair is shown in Figure 2.3. The gears in this study were made of heat-treated aerospace-grade steel. Super-finishing of the gears as a post-processing reduced the surface roughness by an order of magnitude. This process removes the imprints of grinding lay when the teeth were cut to form the gear, leaving the finished surfaces nearly isotropic. Example surface roughness traces prior and post super-finishing are shown in Figure 2.4.

2.4 Gear Surface Defects

A defect-free gear pair at the nominal design tabulated in Table 2.1 would allow operation that is free of failures (tooth bending, contact fatigue, and scuffing) under normal intended conditions. The gears were first measured to qualify that their intended dimensions were within the specified tolerance bands. These qualified gear specimens were then sent out to a third-party vendor for application of scratches to active tooth contact surfaces. In order to determine the influence of surface defects on scuffing performance, three otherwise high-quality gears were intentionally scratched. For repeatability, scratches had to be generated in a precise and controlled manner.

Table 2.1: Major gear parameters of the gear pair used in this study.

Parameter	Pinion	Gear
Module [mm]	4.23	
Center Distance [mm]	91.5	
Number of Teeth	17	26
Pressure Angle [deg]	22.5	
Face Width [mm]	14.0	20.4
Root Diameter [mm]	62.8	99.9
Base Diameter [mm]	66.5	101.7
Outside Diameter [mm]	80.0	117.1
Circular Tooth Thickness [mm]	7.8	5.6

Figure 2.3: A pair of spur gear specimens used in this study.

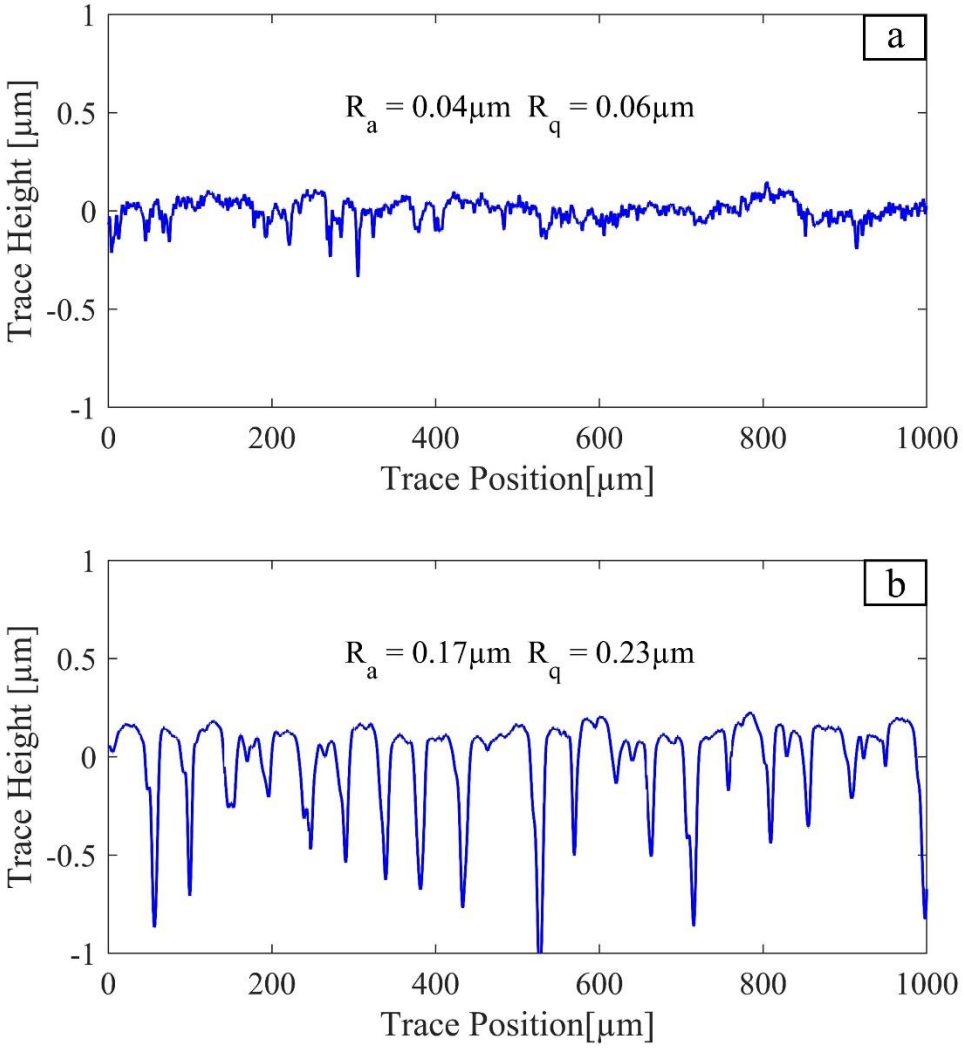

Figure 2.4: Example measured surface roughness traces for (a) super-finished and (b) ground gear specimens.

The gears procured for these tests were case hardened. A sharp (small diameter) tool with a hardness greater than that of the gears was required to generate the scratches. This tool was forced into the gear face in such a manner that the applied normal force with respect to the tooth face and sliding speed were kept constant. This allowed for scratches of a consistent geometry to be generated.

Each scratch was consistent in geometry, but position and orientation on the tooth face were varied. Since the main concern of this study is the determination of scratch tolerability in terms of scuffing performance, contact conditions susceptible to scuffing were of interest. These conditions exist in tooth contact surface areas having both high sliding and high contact stresses. In spur gears with a profile contact ratio less than 2.0, these conditions exist near the highest and lowest points of single tooth contact (HPSTC and LPSTC, respectively). These are the boundaries of the region where only one tooth pair carries the gear mesh force. In other words, they represent the greatest distance (highest sliding) from the operating pitch line where single-tooth contact exists. Figure 2.5 depicts the surface conditions for the highest load, highest speed, and highest temperature test run in this study. The three lines represent the unloaded HPSTC, pitch line, and LPSTC, respectively. The cumulative maximum contact stress distribution p is shown in Figure 2.5(a) at the highest load level, as predicted by a gear load distribution program [23]. In Figure 2.5(b), the sliding velocity $|u_s|$ distribution is plotted at the highest speed condition. The product of the p and $|u_s|$ distributions, $|u_s|\,p$, is given in Figure 2.5(c).

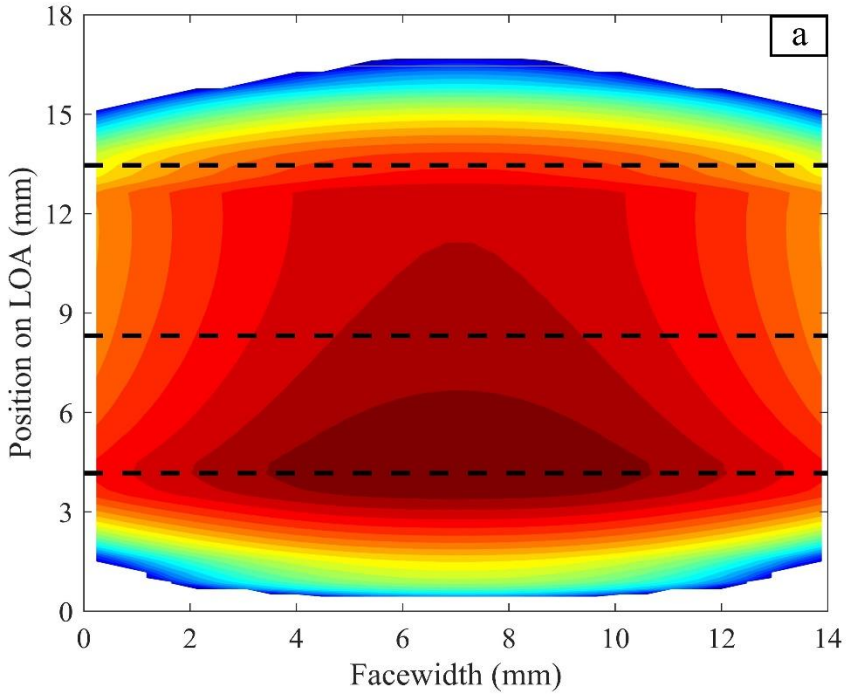

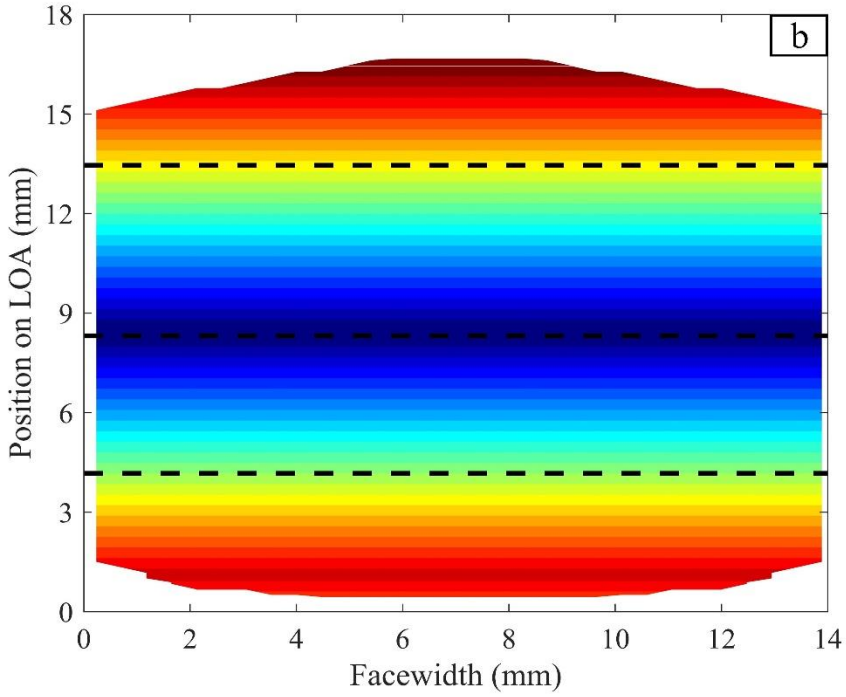

Continued

Figure 2.5: (a) p (b) $|u_s|$, and (c) $|u_s|\,p$ distributions at the highest speed, highest load conditions tested in this study.

Figure 2.5 Continued.

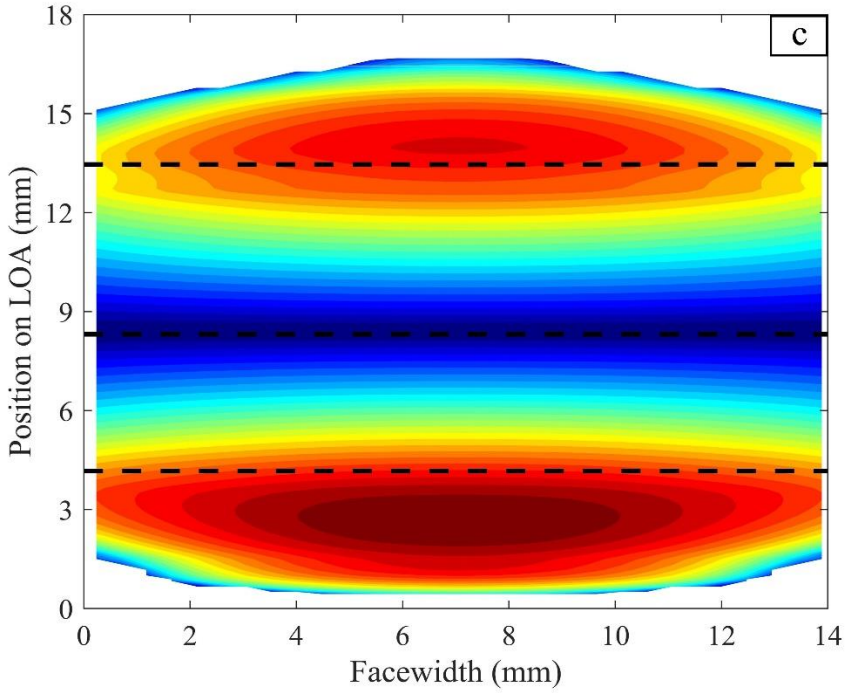

The geometry of each generated scratch is characterized based on the peak-to-valley dimension (H) as shown in Figure 2.6. The other key parameters are defined as the shoulder height (αH), scratch width (βH), and half-shoulder width (γH).

Three pinion gear specimens were altered with scratches at depths of $H \subset [15, 21]$ μm. One pinion was applied with an axial scratch along the LPSTC line, another one had an axial scratch along HPSTC, while the third specimen was scratched diagonally. Table 2.2 lists the measured dimensions of these scratches at their initial (pre-test) states.

Figures 2.7-2.9 show macro and micro images along with a roughness trace of the axially scratched specimen at the LPSTC, the diagonally scratched specimen, and the axially scratched specimen at the HPSTC, respectively. The diagonal scratch covered the entire face width of the gear between the HPSTC line and the pitch line. The contact lines of helical gears are not axially oriented along the tooth profile as is the case for spur gears. Axial scratches are more representative of diagonal scratches on helical-type gears.

2.5 Test Procedure

The scratched pinions, along with a nominal baseline pinion, were put through a staged scuffing protocol to correlate scratch presence with scuffing performance. The generated scratches had significant amounts of material displaced, resulting in the tall, narrow protrusion depicted by αH in Figure 2.6. This shoulder protrusion was measured to be significantly larger (>1 μm) than the oil film thickness under the planned operating

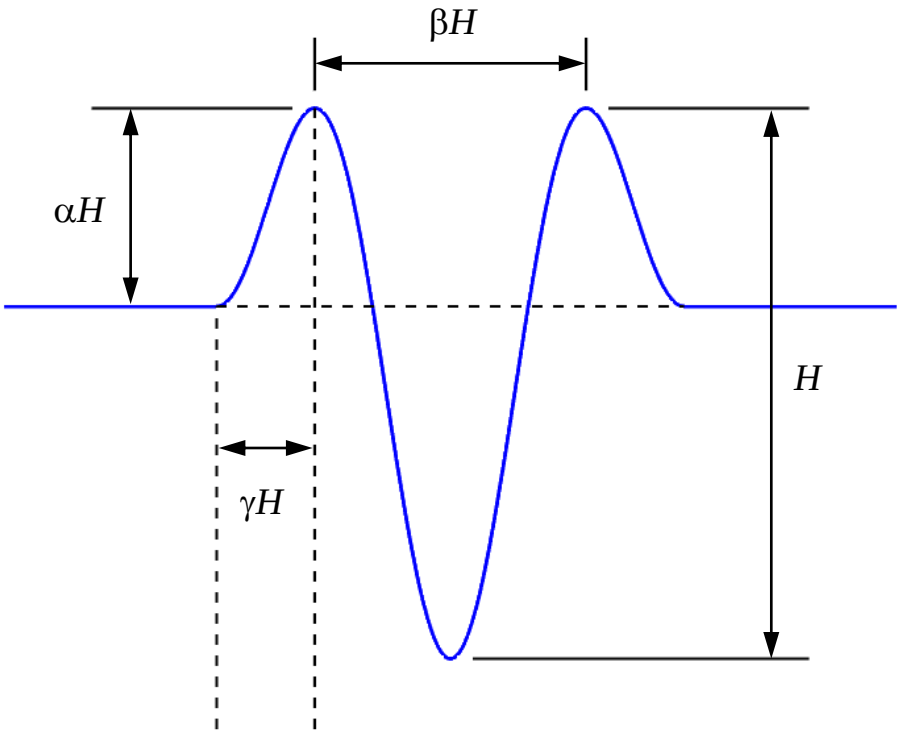

Figure 2.6: Parameterization of a typical scratch.

Table 2.2: Measured initial scratch sizes and geometry parameters.

Scratch Parameter	LPSTC	Diagonal	HPSTC
H [μm]	15	19	21
α	0.11	0.28	0.27
β	4.44	3.79	2.55
γ	0.60	1.01	0.48

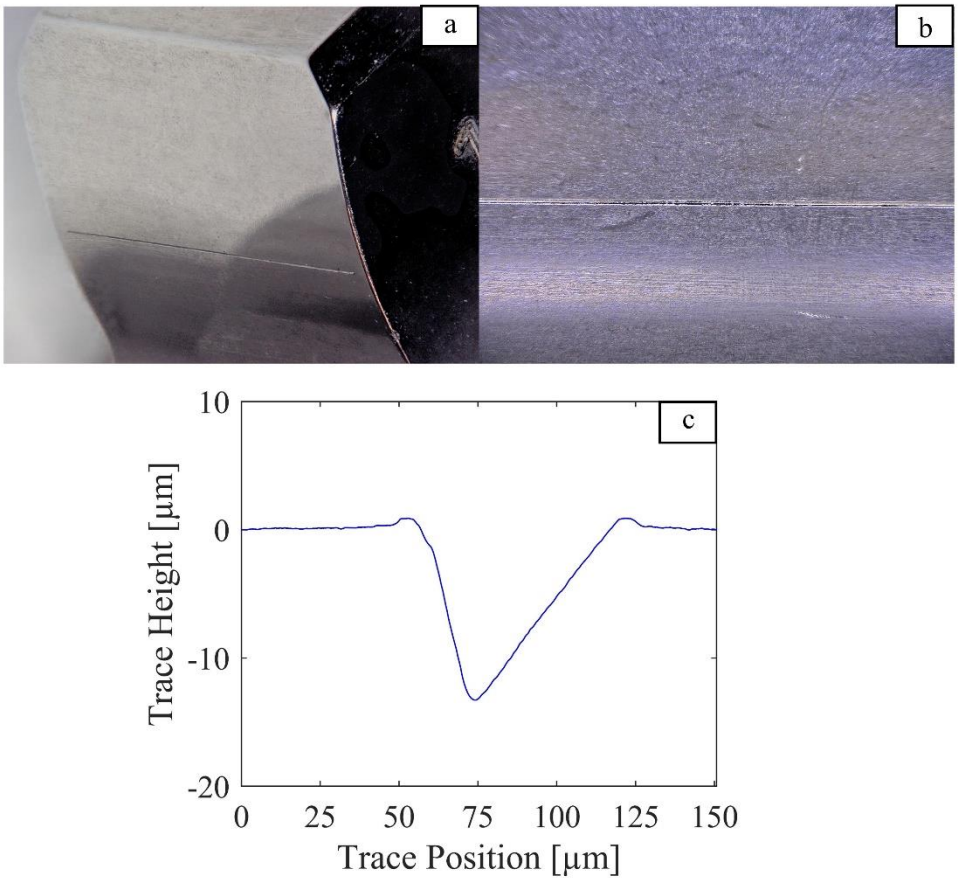

Figure 2.7: (a) Macroscopic image, (b) microscopic image, and (c) roughness trace of the LPSTC scratch tested in this study.

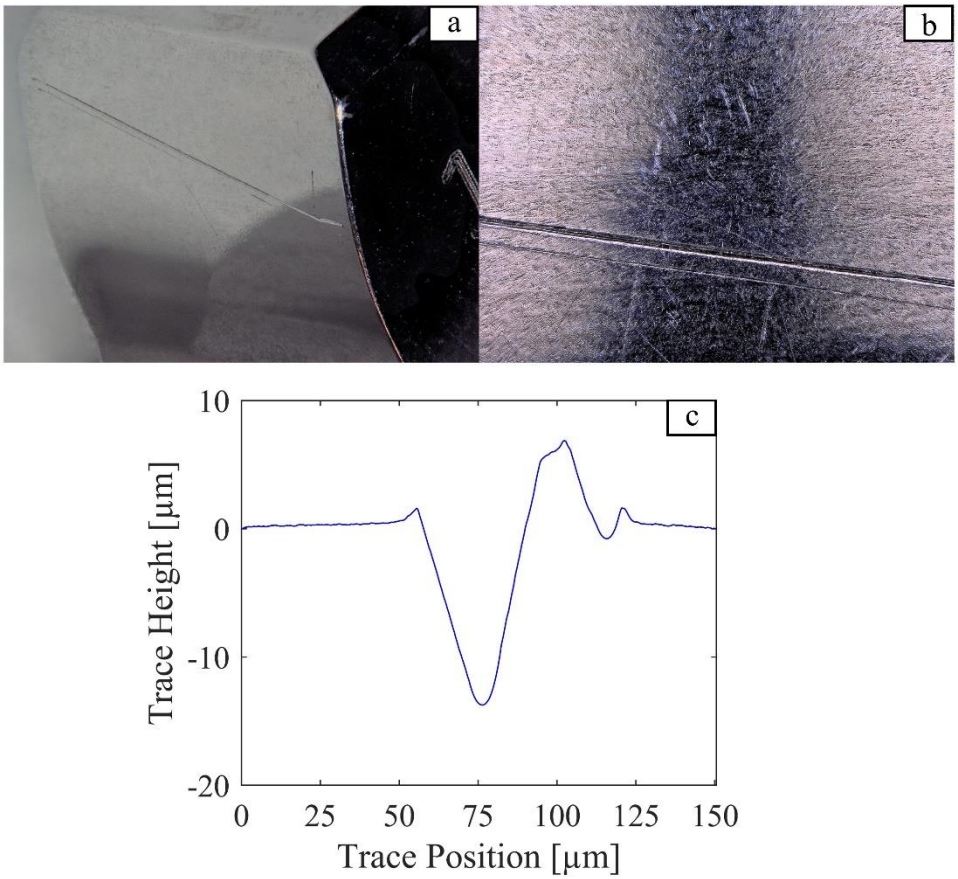

Figure 2.8: (a) Macroscopic image, (b) microscopic image, and (c) roughness trace of the diagonal scratch tested in this study.

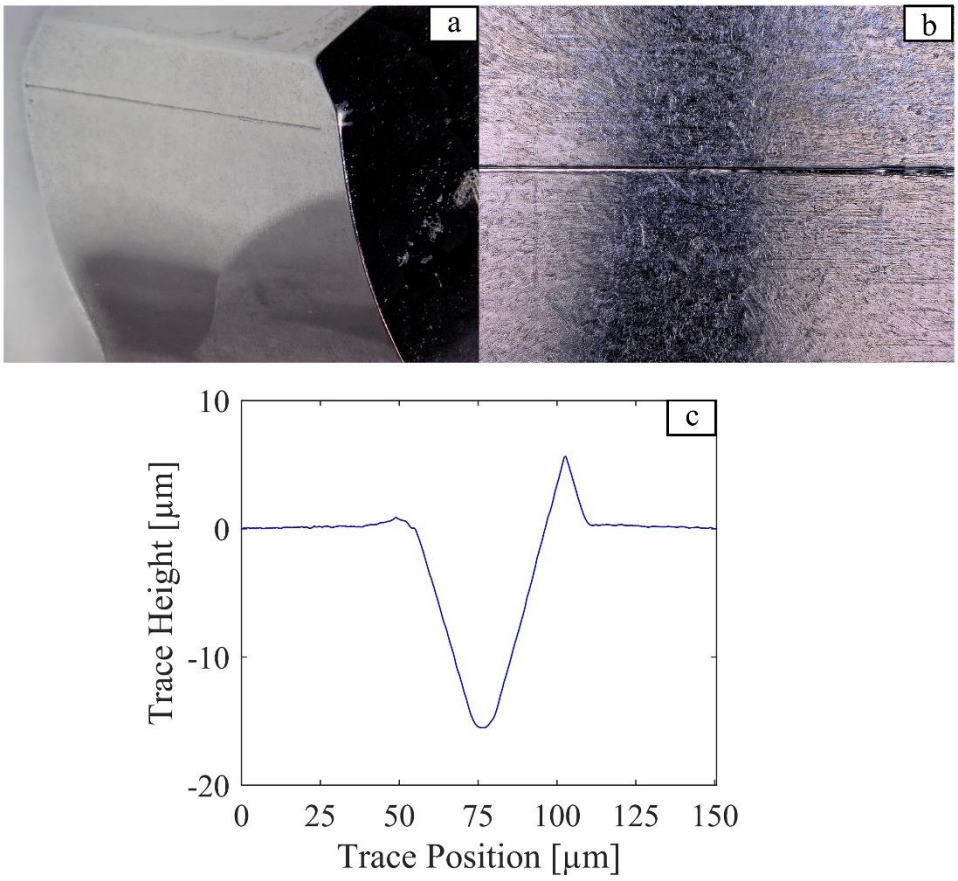

Figure 2.9: (a) Macroscopic image, (b) microscopic image, and (c) roughness trace of the HPSTC scratch tested in this study.

conditions. Such plus material of significant heights is likely to cause debris due to brittle fracture of the shoulder protrusions, causing additional mechanisms for surface damage or premature scuffing failure. Initial run-ins were performed at reduced speeds, torques, and oil temperatures to remove or reduce the height of plus material with minimal surface damage to the tooth. Surface roughness, discoloration of the metal due to bluing or oil, and scratch geometry were all considered when determining the run-in conditions. Run-ins varied for each gear as each defect responded differently to the run-ins. Once the surface wear progression ceased sufficiently, the gears were subjected to the intended aerospace test conditions. The run-ins used for each gear are summarized in Table 2.3.

Once the gears were run in, various aerospace conditions were mimicked on the high-speed machine to test the tolerability of the applied defects. Rotational speed, torque, and inlet oil temperature were all varied. This study used a modified test matrix developed by Lim [21] that incrementally modifies the three independent variables to increase the severity of the operating conditions, as shown in Table 2.4. These conditions were each run for one hour. For confidentiality, the torque defined in Tables 2.3 and 2.4 are normalized.

2.6 Inspection Procedure

Metrological procedures were developed to track surface transformations throughout the staged scuffing tests. Measurements were conducted initially and after each tested stage, including run-ins. The measurements performed included contact-type surface roughness traces, gear coordinate measurements (CMM), and microscope imagery.

Table 2.3: Run-in summary for each tested gear pair.

	Oil Temp [°C]	Speed [rpm]	Torque	Time [min]	Gears Run
Stage 1	50	100	0.24T	1	HPSTC LPSTC Diagonal
Stage 2	50	100	0.24T	10	HPSTC LPSTC Diagonal
Stage 3	132	8000	T	2.5	HPSTC LPSTC
Stage 4	132	8000	T	15	HPSTC

Table 2.4: Scuffing test matrix performed in this study.

Scuffing Stage	Oil Temp [°C]	Speed [rpm]	Torque
A1, A2, A3		8,000	T, 1.11T, 1.31T
A6	132	10,000	1.31T
A9		12,000	1.31T
B1, B2, B3		8,000	T, 1.11T, 1.31T
B6	141	10,000	1.31T
B9		12,000	1.31T
C1, C2, C3		8,000	T, 1.11T, 1.31T
C6	149	10,000	1.31T
C9		12,000	1.31T

Contact-type surface roughness traces provide a two-dimensional cross-sectional measurement of the surface. These measurements were used to track scratch geometry and surface roughness throughout the tests. Four traces were taken in both the axial and profile directions of the tooth for a total of eight traces in four locations to monitor surface profile changes away from the defects. Measurements were conducted on a Form Talysurf 60. These measurements were subject to a band-pass filter removing all features with wavelengths outside of 0.01 to 0.0001 thousandths of an inch according to Ref. [24]. This allowed the retention of surface roughness features, while removing form features such as the involute profile of the gear. For measuring the geometry of the scratch, the facewidth of the pinion was divided into seven sites approximately 2 mm wide. A probe roughness trace of each scratch was performed at the center of each site. Filtration was not performed on the scratch to maintain its measured geometry.

Gear CMM measurements were conducted on a Klingelnberg P26. Measurements were taken prior to testing in order to ensure that the correct macro and micro geometries were applied to each gear. Tooth topography was documented for four teeth evenly spaced around the gear for both profile and lead directions. Tooth-to-tooth spacing errors were also measured.

High-resolution imagery was the backbone of the inspection procedure. Microscope images taken of the gear were performed on two different lenses using a Keyence VHX-6000. A macroscopic lens was used at 30X zoom to capture the entire tooth surface, while a high-magnification lens was used to capture images at 100X, 300X, and 1000X magnification. Several sites along the scratch were tracked between stages of

running to assess the surface damage acquired throughout the stage. Any other large abnormalities were documented and monitored throughout the testing procedure.

2.7 Summary

A high-speed gear test set-up was introduced to be used in tests of gears having scratches. Key mechanical, instrumental and lubrication features of the test machine were described. The baseline geometries of the spur gear specimens were defined. The three types of scratches applied, LPSTC, HPSTC and diagonal, were introduced and parameterized. Inspection procedures and a staged gear test protocol were defined and described. The tests and inspection procedures performed according to this protocol will be presented in the next chapter.

CHAPTER 3

EXPERIMENTAL GEAR SCUFFING PERFORMANCE

3.1 Introduction

The influence of surface defects in the form of scratches on gear scuffing performance was investigated according to the procedures outlined in Chapter 2. The results of this investigation are presented in this chapter. First, a gear pair with no apparent defects was tested. This was done to establish a baseline for surface degradation that can be expected under normal conditions. The results for the intentionally scratched pinions followed, with scratches at the locations of the lowest point of single tooth contact (LPSTC) line, diagonal between the highest point of single tooth contact (HPSTC) and the pitch line, and along the HPSTC line being presented.

3.2 Staged Scuffing Experiments

Scratch geometry varied with axial position since the scratches were not generated perfectly uniform. While measurements across a scratch were made at the same intended locations, even minor deviations in location were seen to result in apparent inconsistencies in scratch geometry. The measurements illustrate scratches that appear to grow, warp, or

shrink slightly. As such, while the changes in the areas of plus material are real, minor variations along the valley of the scratch should be viewed to be a result of measurement location inconsistency.

3.2.1 A Damage-Free Gear Pair

This study made use of specimens fabricated to an existing gear design for high-speed gear testing as in several earlier studies[11–13,21]. Without modification, these gears are expected to pass the proposed staged scuffing test defined in Table 2.4 without failure. To establish a typical level of surface distress, an undamaged gear pair was considered first.

Figure 3.1 shows the pinion reference tooth from the undamaged tests after scuffing stages A1, A2, A3, A9, B9 and C9. Various areas of discoloration and apparent damage are seen to accumulate with each scuffing stage. While most of these were superficial, one gouge was observed in the left addendum of the pinion after stage A3 (Figure 3.1(c)). This gouge progressed slowly before causing a sizable scuffing zone in the same area during stage C9 as shown in Figure 3.1(f). Stage C9 was halted prematurely due to a sharp increase in vibrations caused by scuffing. Table 3.1 lists the operating conditions of stage C9 as the failure stage for this test.

For inspection purposes, the pinion tooth surface was divided into seven sections along its face width. Inspections could be performed within each section at the roll angles of the LPSTC and/or HPSTC, corresponding to a total of 14 possible inspection locations.

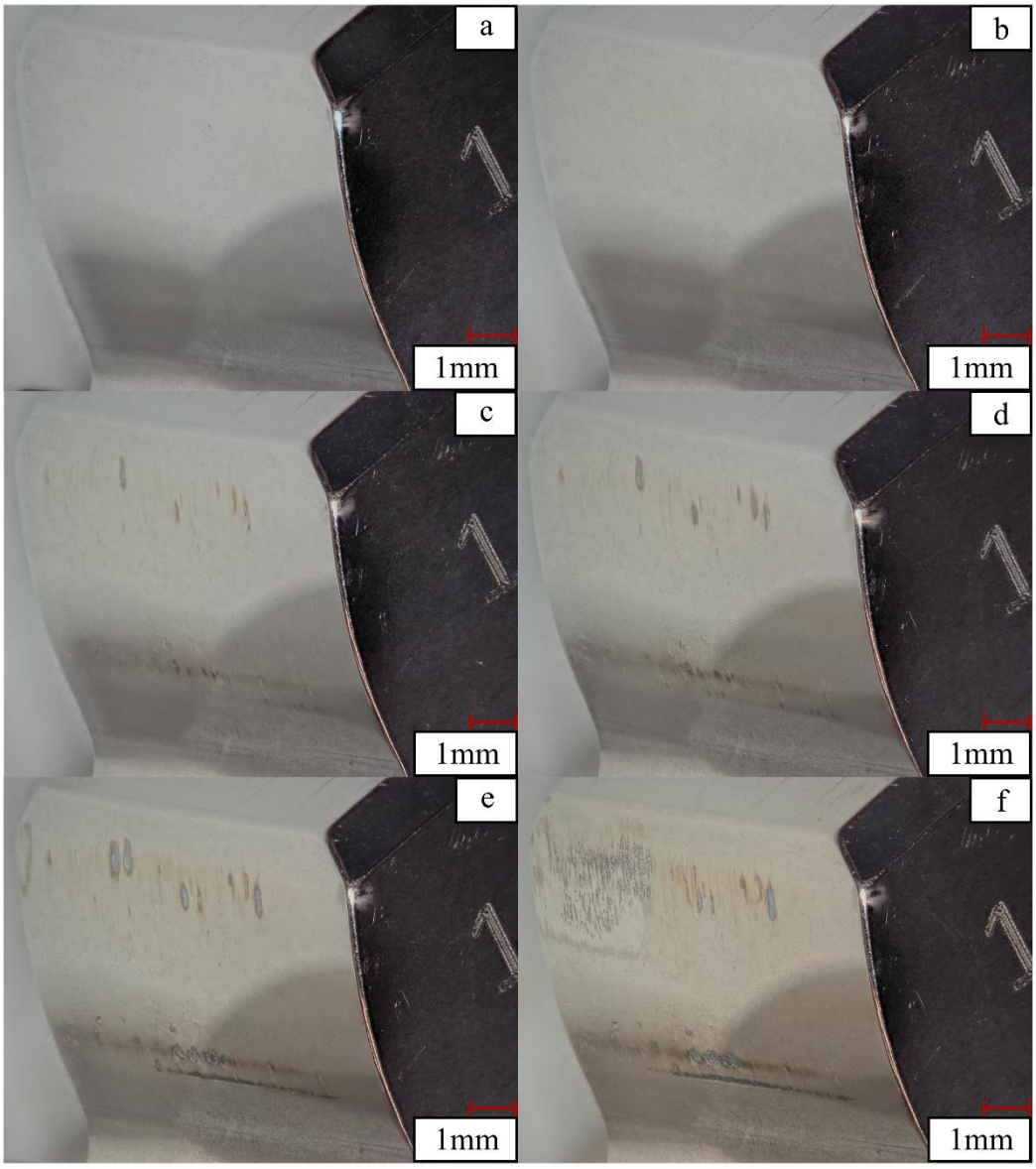

Figure 3.1: Macro-images of the pinion tooth having no scratch in site 4 (a) before the test, and after the stages of (b) A1 (c) A3, (d) A9, (e) B9, and (f) C9.

Table 3.1: Summary of staged scuffing test results.

	Operating Conditions at Failure		
Gear Pair	Oil Temp [°C]	Speed [rpm]	Torque
No Damage	149	12,000	1.31T
LPSTC	132	8,000	1.31T
Diagonal	132	8,000	1.31T
HPSTC	132	12,000	1.31T

Inspections were performed on the tooth surface of interest after the completion of each scuffing stage. These axial sections were numbered 1 through 7 from left to right. For the sake of brevity, only section 4 will be presented, representing the mid-plane of the gears. Additionally, not all test stages are displayed. Microscope images for the undamaged pinion within section 4, taken at 300X magnification, are shown in Figures 3.2 and 3.3 at the HPSTC and LPSTC locations, respectively.

Some debris-induced scratches and localized hot spots are evident in Figure 3.2, mostly in the addendum area of the pinion. In addition, the contact areas of gear tip and pinion dedendum show signs of distress as seen in Figure 3.3.

3.2.2 A Gear Pair Having a LPSTC Scratch on the Pinion

The first damaged gear pair to be run used a pinion scratched along its LPSTC line. This gear pair was first run through three run-in stages. It subsequently survived the first two scuffing stages before scuffing at stage A3, as listed in Table 3.1. Figure 3.4 shows roughness traces across this scratch at section 4 (middle of the tooth) in its pre-test form as well as after run-in and staged tests. Focusing on the pre-test scratch profile (blue line), the dimensional parameters of this scratch as defined in Figure 2.6 were $H = 15$ μm, $\alpha = 0.11$, $\beta = 4.44$, and $\gamma = 0.60$. The small α value indicates that the plus material initially present along the edges of the scratch was minimal. Traces performed after run-in and staged tests do not exhibit any plus material as they wore out during the run in Otherwise, the overall shape of the scratch remained relatively unchanged during the tests.

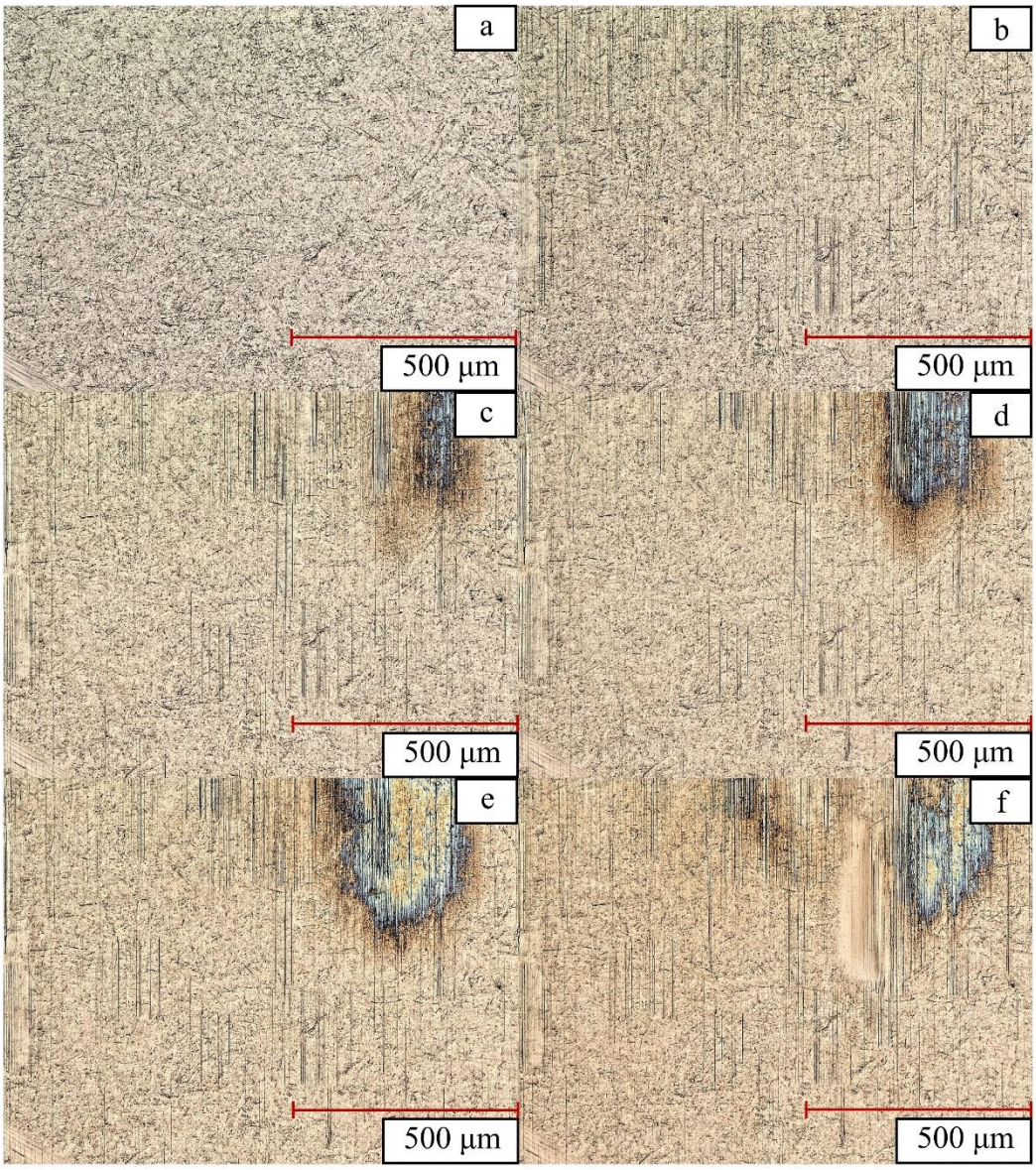

Figure 3.2: 300X images of the pinion tooth having no scratch in HPSTC areas of site 4 (a) before the test, and after the stages of (b) A1 (c) A3, (d) A9, (e) B9, and (f) C9.

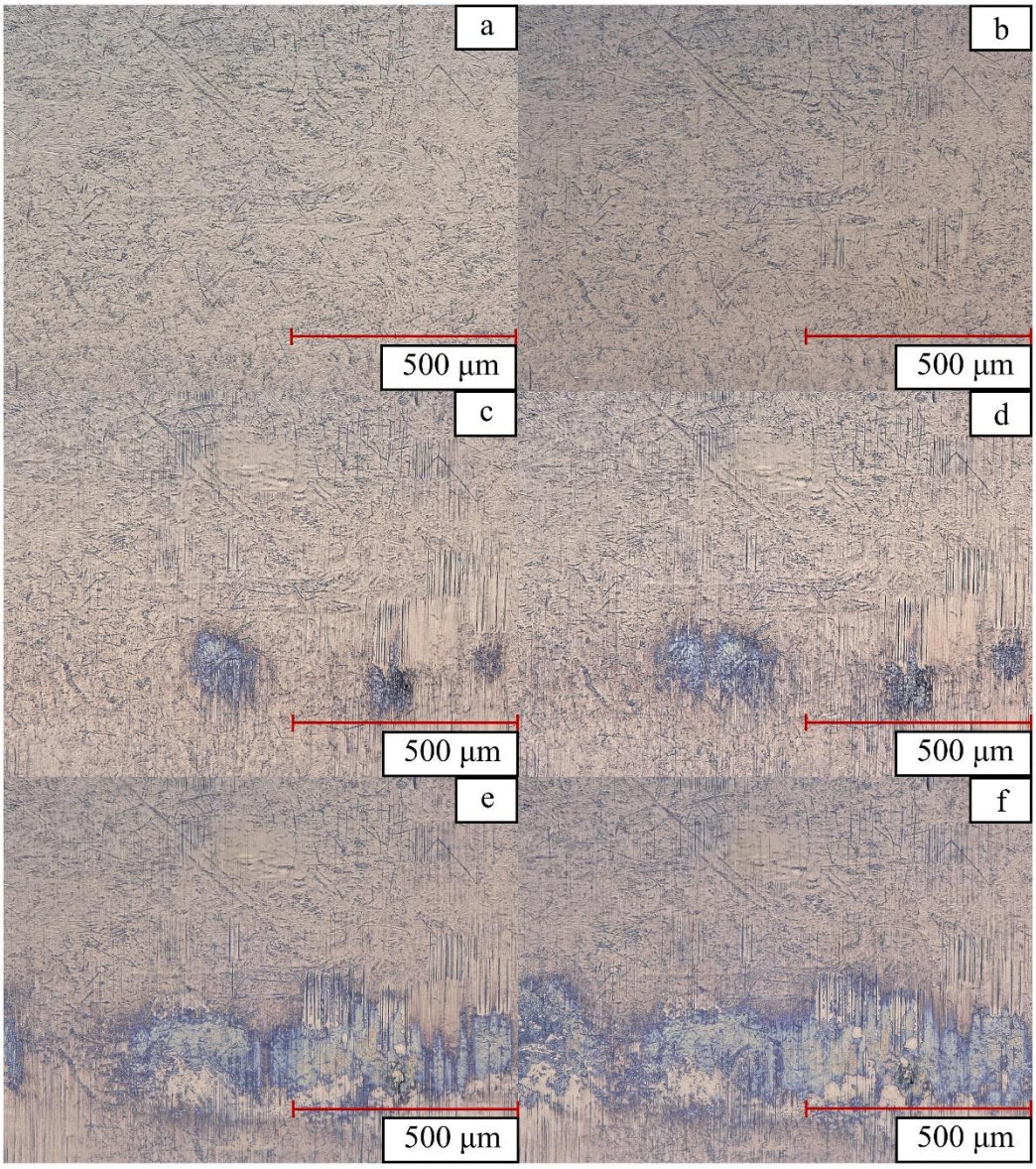

Figure 3.3: 300X images of the pinion tooth having no scratch in LPSTC areas of site 4 (a) before the test, and after the stages of (b) A1 (c) A3, (d) A9, (e) B9, and (f) C9.

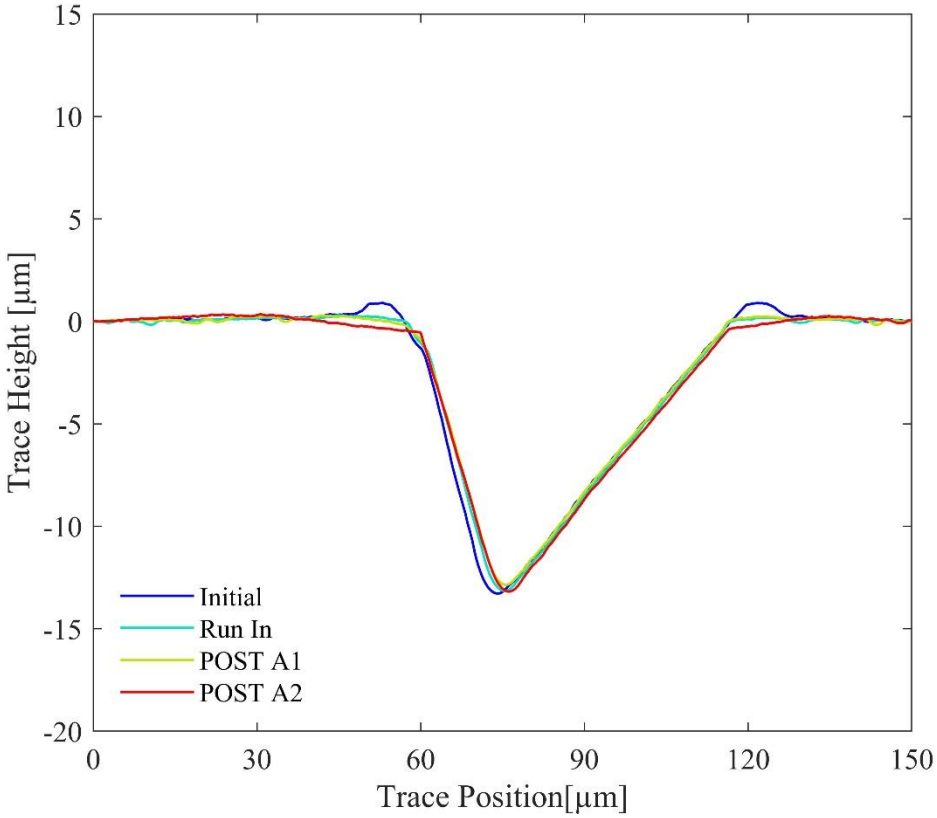

Figure 3.4: Roughness profiles of the LPSTC scratch at site 4.

Figure 3.5 shows the entire pinion tooth having the LPSTC scratch at pre-test and after run-in and scuffing test stages. While the tooth surface is seen to maintain its integrity all the way to the end of stage A2 (Fig. 3.5(d)), a band of scuffing marks covering the entire face width along the dedendum is evident in Figure 3.5(e). 100X close-up views of the scratched area within section 4 are shown in Figure 3.6. Very little or no changes are observed along the scratch after various test stages. Furthermore, the scuffing region in Figure 3.6(e) after stage A3 is clearly below the scratch with no conclusive evidence that the scratch might have induced the scuffing failure.

The magnified (1000X) images of the scratch at the same section are presented in Figure 3.7 after run-in and the three scuffing stages. As the gear pair was run, the shoulders developed smooth regions on both sides of the scratch, free from the surface features present on the rest of the tooth surface. The size of the zone increased in the profile direction as the gear pair was run-in, and then remained relatively steady in size until failure. The smoothened region on the lower shoulder was observed to be somewhat wider than that of the upper shoulder. Figure 3.7(b) shows some discoloration below the scratch shoulder in the direction of sliding that developed after run-in. It continued to develop further until scuffing failure in stage A3 (Figure 3.7(e)). This discoloration is a likely indication of bluing of the gear steel due to heat buildup combined with formation of a tribofilm (gold-brown discoloration) due to lubricant additives.

A small damage zone was observed after stage A2, as shown in Figure 3.8. It featured both finite-length micro-scratches and smooth regions extending below the

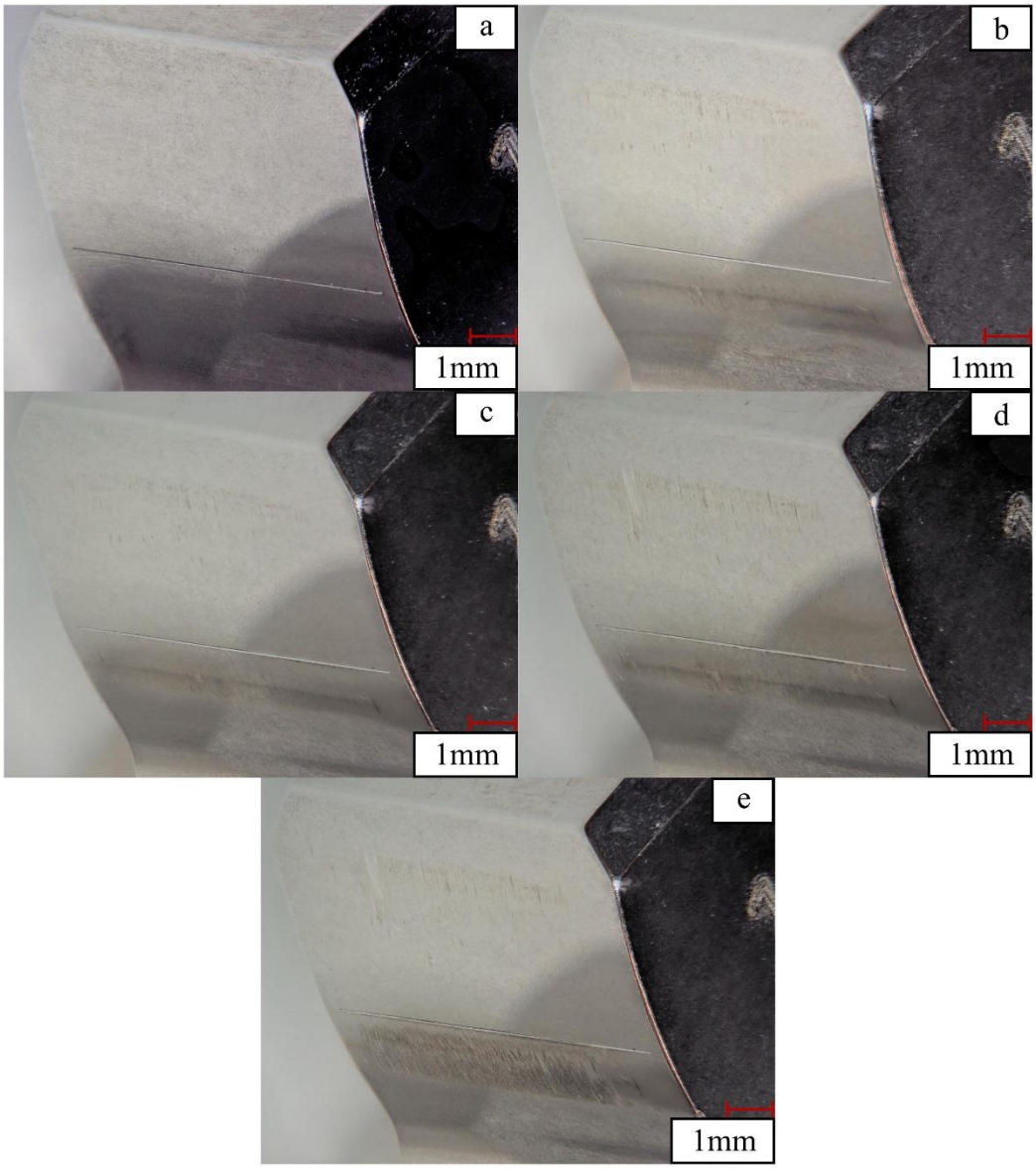

Figure 3.5: Macro-images of the pinion tooth having the LPSTC scratch in site 4 (a) before the test, and after the stages of (b) run-in, (c) A1, (d) A2, and (e) A3.

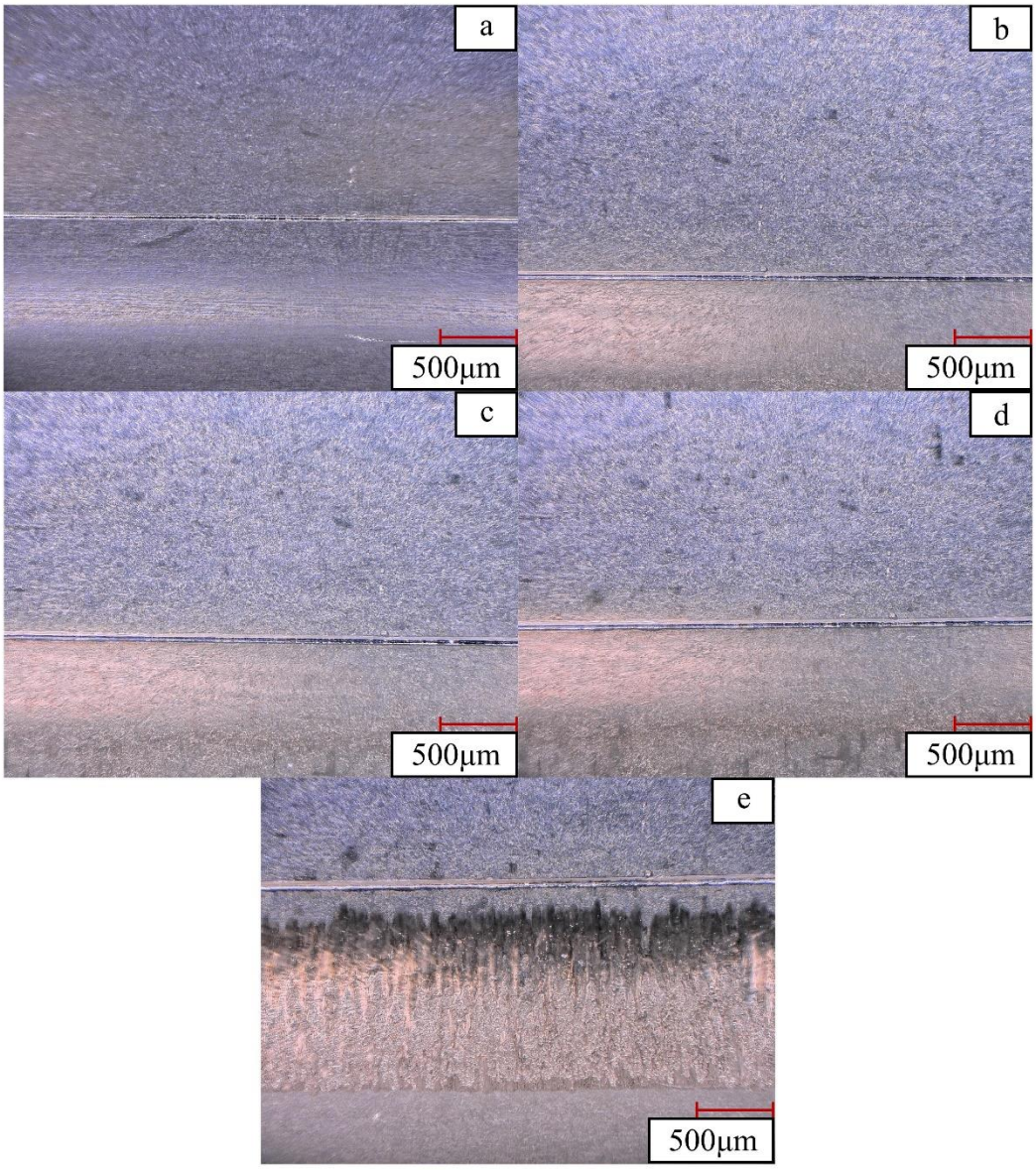

Figure 3.6: 100X microscopic of the LPSTC scratch in site 4 (a) before the test, and after the stages of (b) run-in, (c) A1, (dc) A2, and (e) A3.

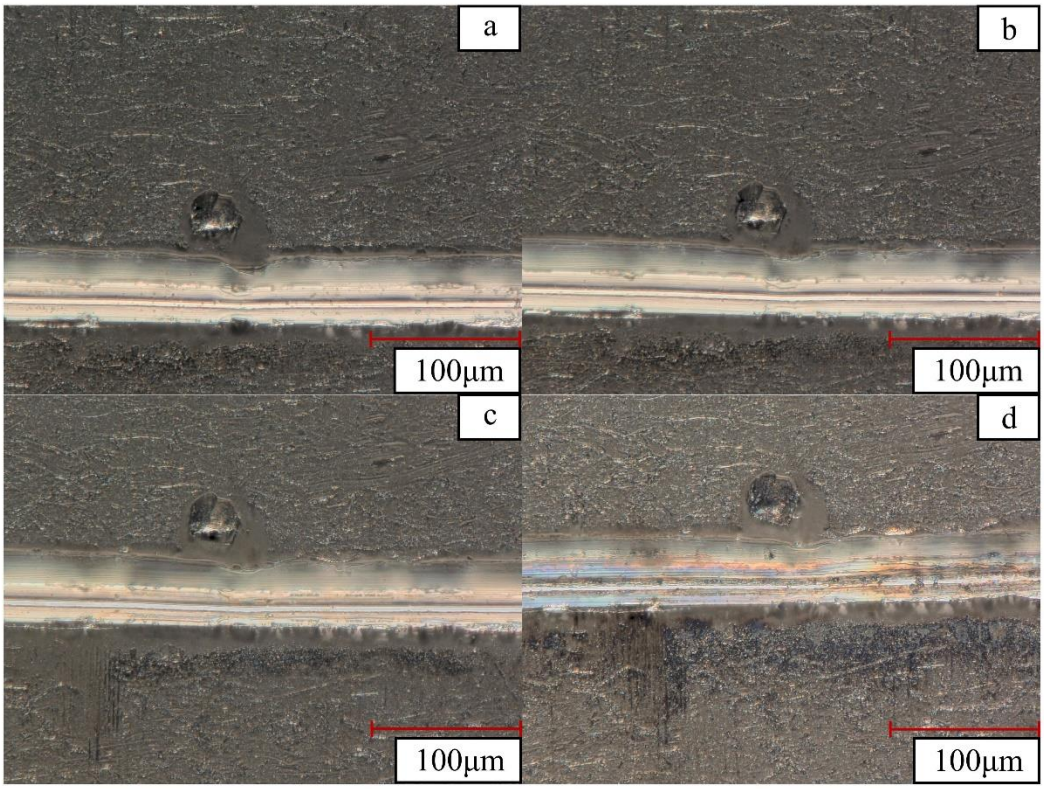

Figure 3.7: 1000X images of the LPSTC scratch in site 4 after (a) run-in, (b) stage A1, (c) stage A2, and (d) stage A3.

Figure 3.8: A damage zone near the LPSTC scratch (400X magnification).

induced scratch. It is possible that these micro-scratches were caused by small debris particles being removed from the shoulders, finding their way to the oil supply, and passing through the contact zone.

Although the scuffing failure region shown in Figures 3.5(e) and 3.6(e) was clearly separated from the scratch, it can still be hypothesized that the failure is still caused by the scratch indirectly through additional heat and loose debris caused by it.

3.2.3 A Gear Pair Having a Diagonal Scratch on the Pinion

The third tested gear pair consisted of a pinion with an intentional diagonal scratch spanning from the HPSTC line at one side of the face width to the pitch line on the other. As applying a diagonal scratch of precise dimensions and trajectory is more challenging, the resultant diagonal scratch was found to consist of two parallel scratches. Figure 3.9 shows a roughness profile across this scratch in section 7 along the radial direction. At the left hand side of this figure, there is a scratch having parameters $H = 19$ μm, $\alpha = 0.28$, $\beta = 2.53$, and $\gamma = 0.40$. To the right of this scratch at a valley-to-valley distance of about 45 μm, another scratch is present at parameters $H = 12$ μm, $\alpha = 0.16$, $\beta = 3.00$, and $\gamma = 0.50$. While this double-scratch condition was not intended, it was still found relevant here as most real-life scratches on gears have similar features.

This gear pair also failed during scuffing stage A3 as listed in Table 3.1. Figure 3.10 shows images of the scratched tooth in its pre-test form as well as after run-in and scuffing stages A1, A2 and A3. It is clear from Figure 3.10(e) that there is a band of

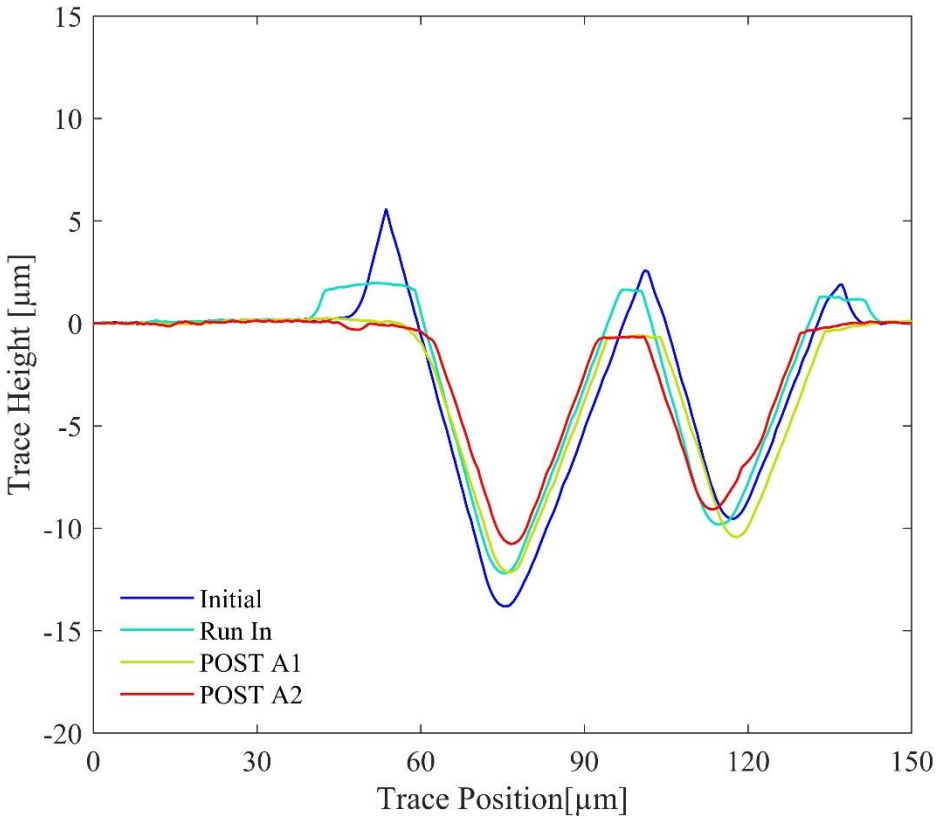

Figure 3.9 Roughness profiles of the diagonal scratch at site 7.

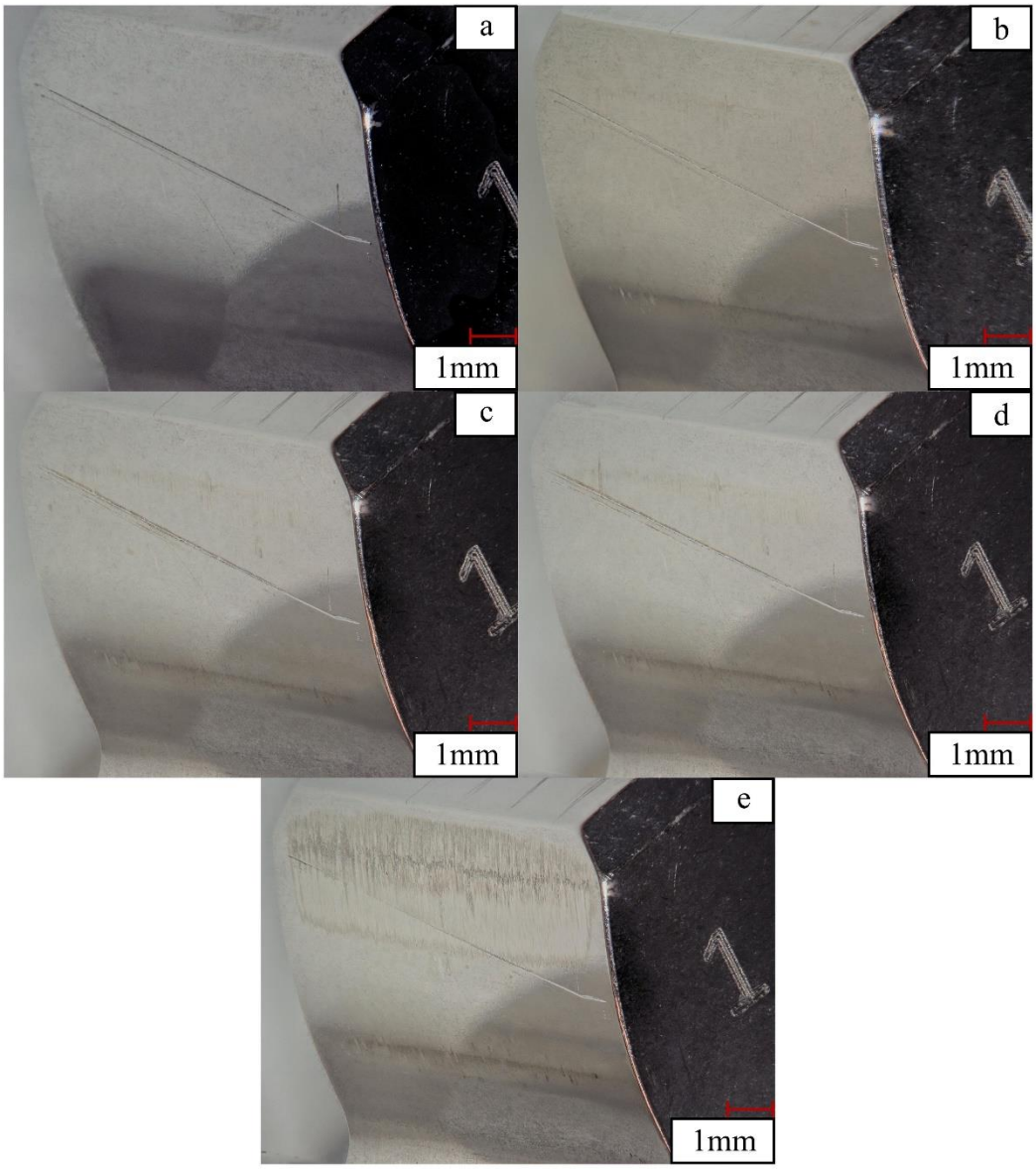

Figure 3.10: Macro-images of the pinion tooth having a diagonal scratch in site 4 (a) before the test, and after the stages of (b) run-in, (c) A1, (d) A2, and (e) A3.

scuffing in the addendum of the pinion while it did not exist in Figure 3.10(d) after stage A2. Yet, Figure 3.10(d) has conclusive evidence that the first scuffing mark was initiated at the diagonal scratch at site 2 going towards the tip. Figure 3.11 show a close-up image of this early scuffing site originating from the scratch. The shoulders of these scratches with plus material are seen to be flattened at site 7 after stage A1 as shown in Figure 3.9.

Figures 3.12 and 3.13 present magnified images of the diagonal scratch in section 4 after various stages of the test. It is seen in these images that the shoulder at the higher roll angle is smeared upwards while the leading shoulder in the bottom is either plastically deformed towards the center of the scratch or broken off in segments. Figures 3.12(e) and 3.13(e) also show the severity of the scuffing and its interaction with the scratch.

Discoloration was also present on and around the shoulders of the scratch. It began after run-in stage two and progressed until scuffing failure during stage A3. The extent of the discoloration was revealed in Figure 3.13(d) after stage A2 when the incidence angle of the microscope was changed to contrast this discoloration better. The bluing appears to be more extensive than the LPSTC scratch. The bluing was also more severe at the axial center of the tooth where contact pressure is highest.

3.2.4 A Gear Pair Having a HPSTC Scratch on the Pinion

The final damage-induced gear pair to be tested had a pinion with axial scratch damage along its HPSTC line. Figure 3.14 shows roughness traces across this scratch at section 4 in its pre-test form as well as after run-in and staged tests. Focusing on the pre-

Figure 3.11: Scuffing initiation site along the diagonal scratch in site 2 after stage A2 (300X magnification).

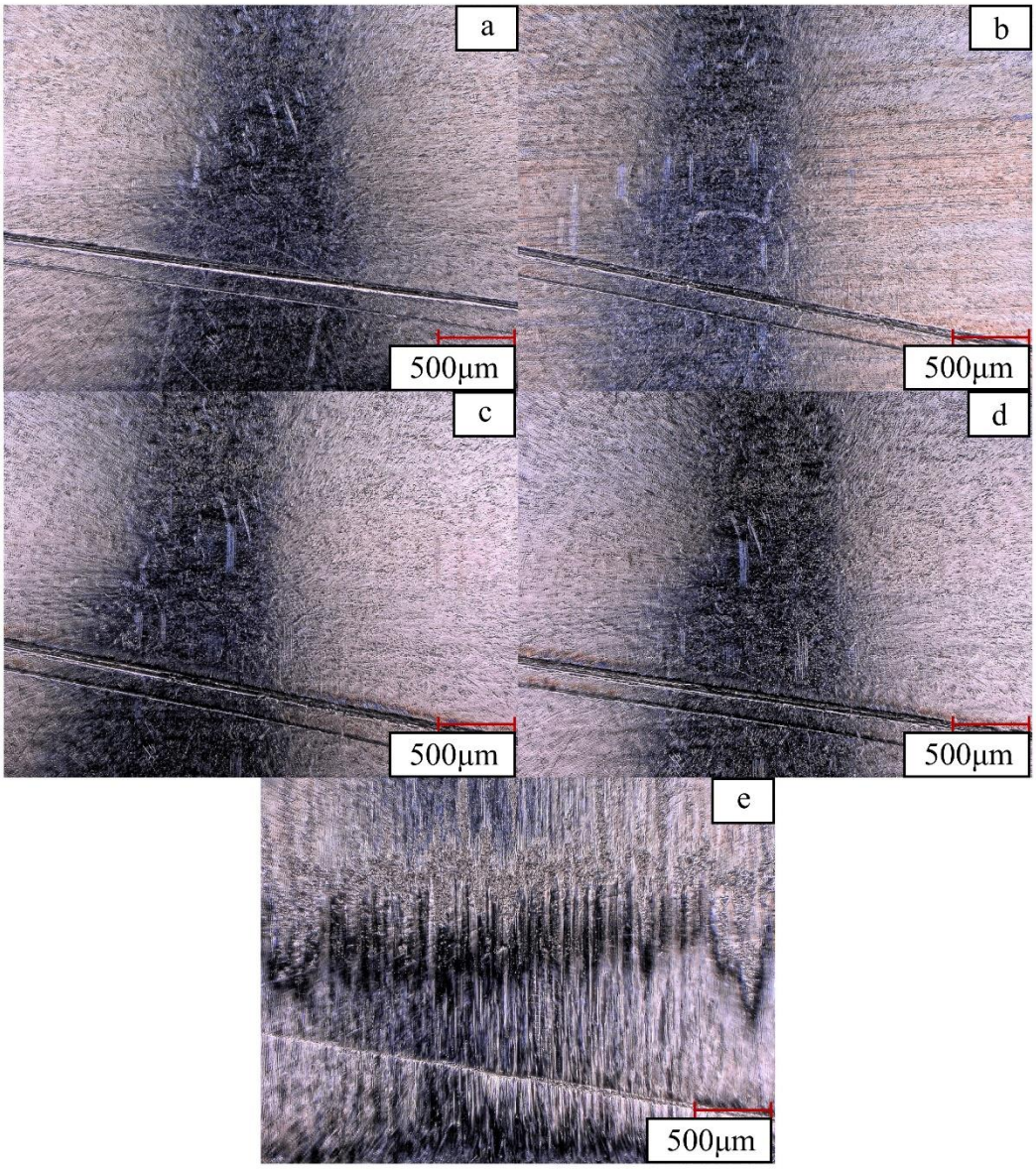

Figure 3.12: 100X microscopic images of the diagonal scratch in site 4 (a) before the test, and after the stages of (b) run-in, (c) A1, (d) A2, and (e) A3.

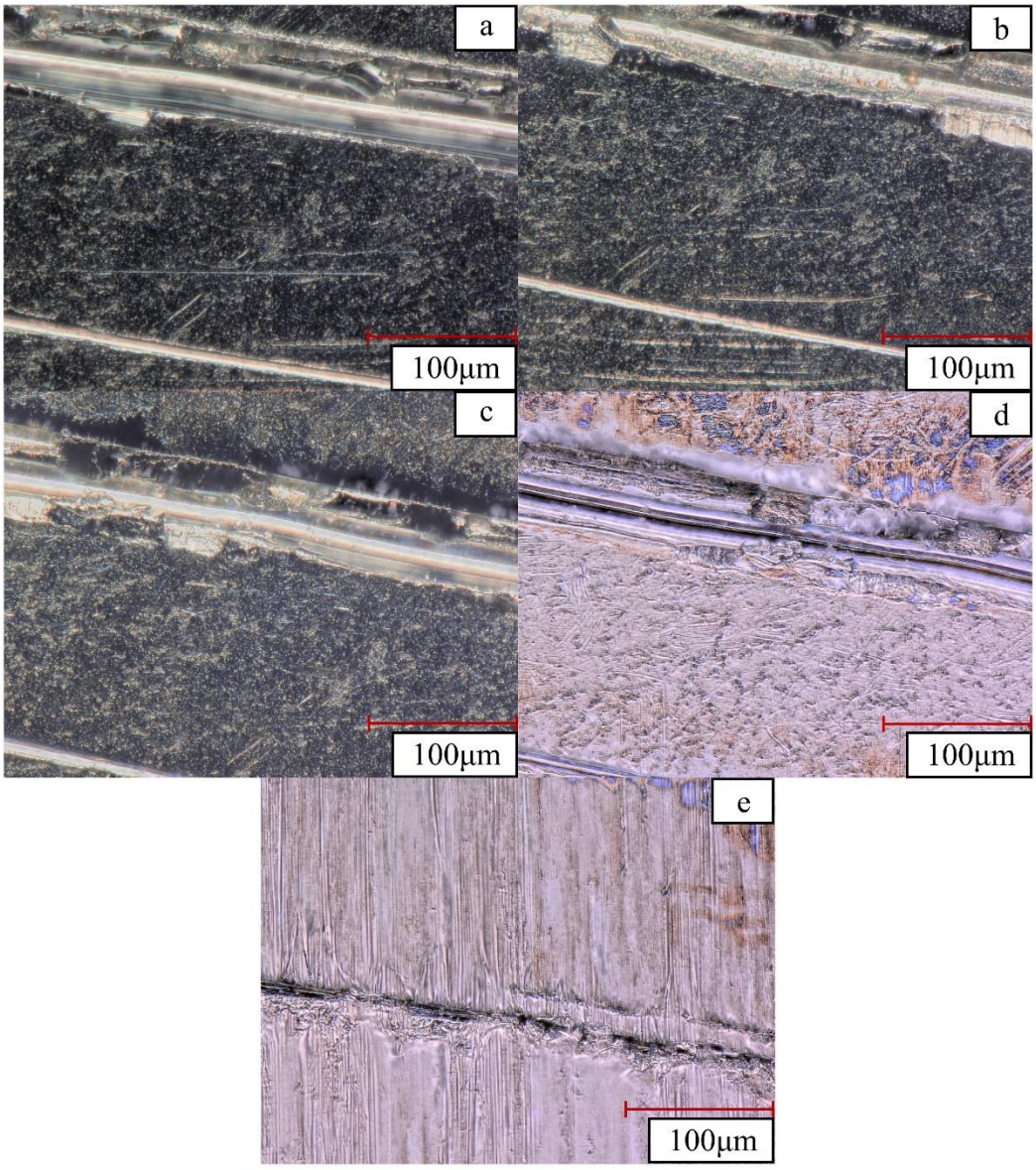

Figure 3.13: 1000X microscopic images of the diagonal scratch in site 4 (a) before the test, and after the stages of (b) run-in, (c) A1, (dc) A2, and (e) A3.

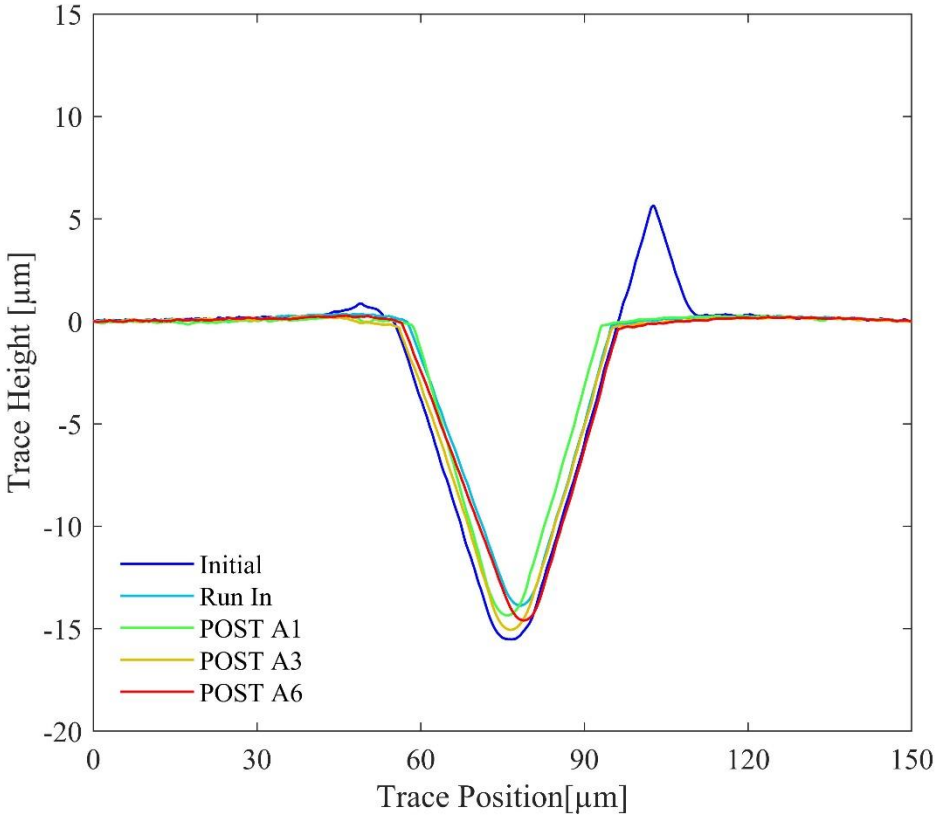

Figure 3.14: Roughness profiles of the HPSTC scratch at site 4.

test scratch profile (blue line), the dimensional parameters of this scratch where $H = 21$ μm, $\alpha = 0.27$, $\beta = 2.55$, and $\gamma = 0.48$. This gear pair was run through four run-in stages before the staged scuffing test. The plus material on the scratch shoulder is seen to wear off completely after the run-in stage. This test was then run through the staged scuffing test and failed during stage A9, as listed in Table 3.1. The pinion tooth with the scratch is shown in Figure 3.15, including pre-test, after run-in, and stages A1, A2, A3 and A9. In Figure 3.15(e) after stage A9, the pinion tooth is shown to exhibit severe addendum and dedendum scuffing. In addition, severe discoloration along the HPSTC scratch is also evident after earlier stages. 100X and 1000X images of the scratch zone at the same test stages are shown in Figure 3.16 and 3.17, respectively. The bluing again occurs after the scratch in the direction of sliding and is most severe at the facewidth center of the tooth. This suggests that the bluing is caused by increased contact pressure, potentially resulting in asperity interactions. This is complemented by Figure 3.17 where a wide flattened zone is observed above the scratch. Otherwise, no initiation sites or scuffing cells were observed. Despite an initiation site not being captured, there is sufficient evidence from the damage visible in Figures 3.16(d) and 3.17(d) to suggest that the reason for this failure was the HPSTC scratch.

3.3 Summary

A total of four gear experiments were performed under realistic high-speed conditions suitable for scuffing failures. They included an undamaged gear pair intended

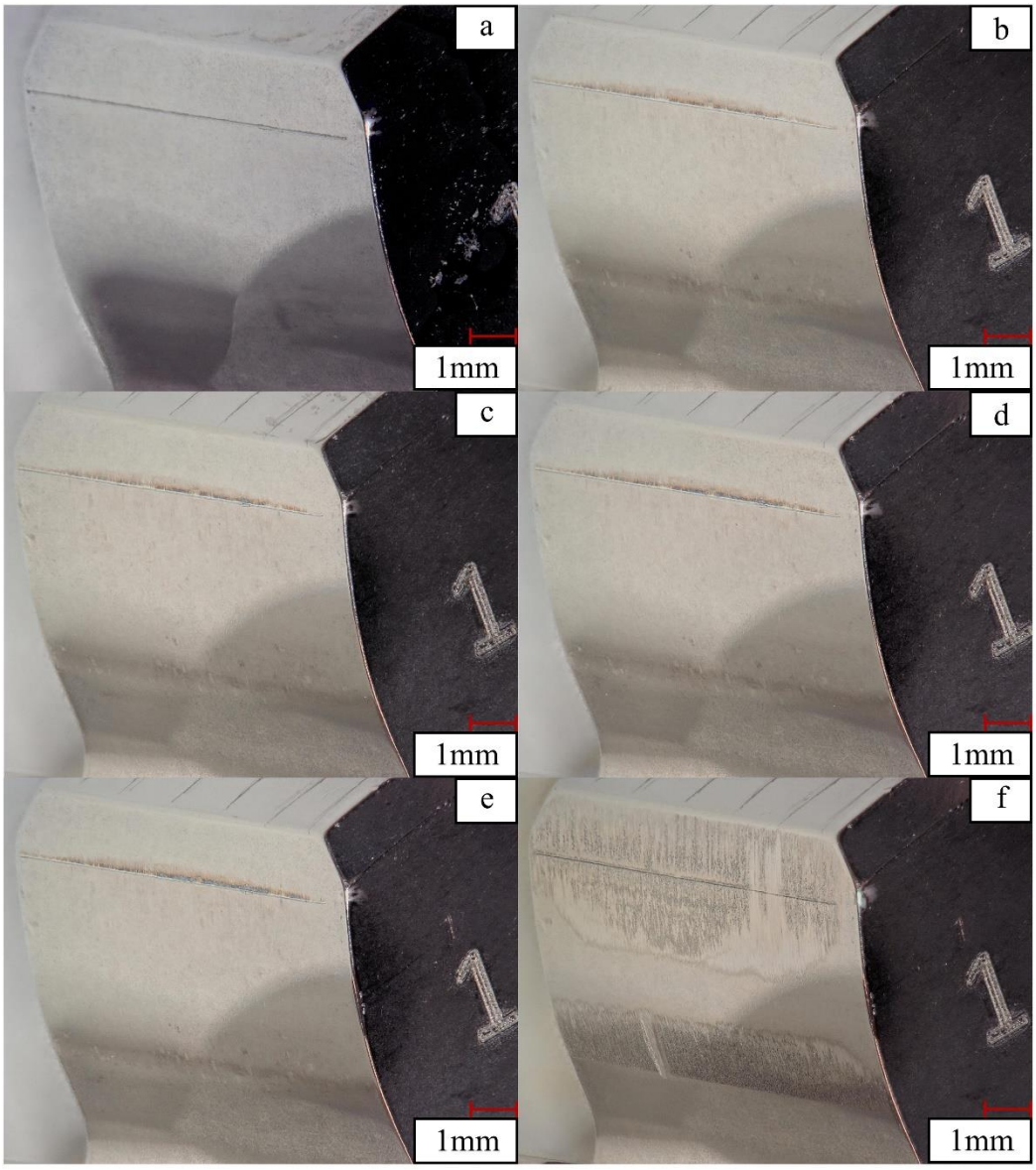

Figure 3.15: Macro-images of the pinion tooth having the HPSTC scratch in site 4 (a) before the test, and after the stages of (b) run-in, (c) A1, (d) A2, (e) A3, and (f) A9.

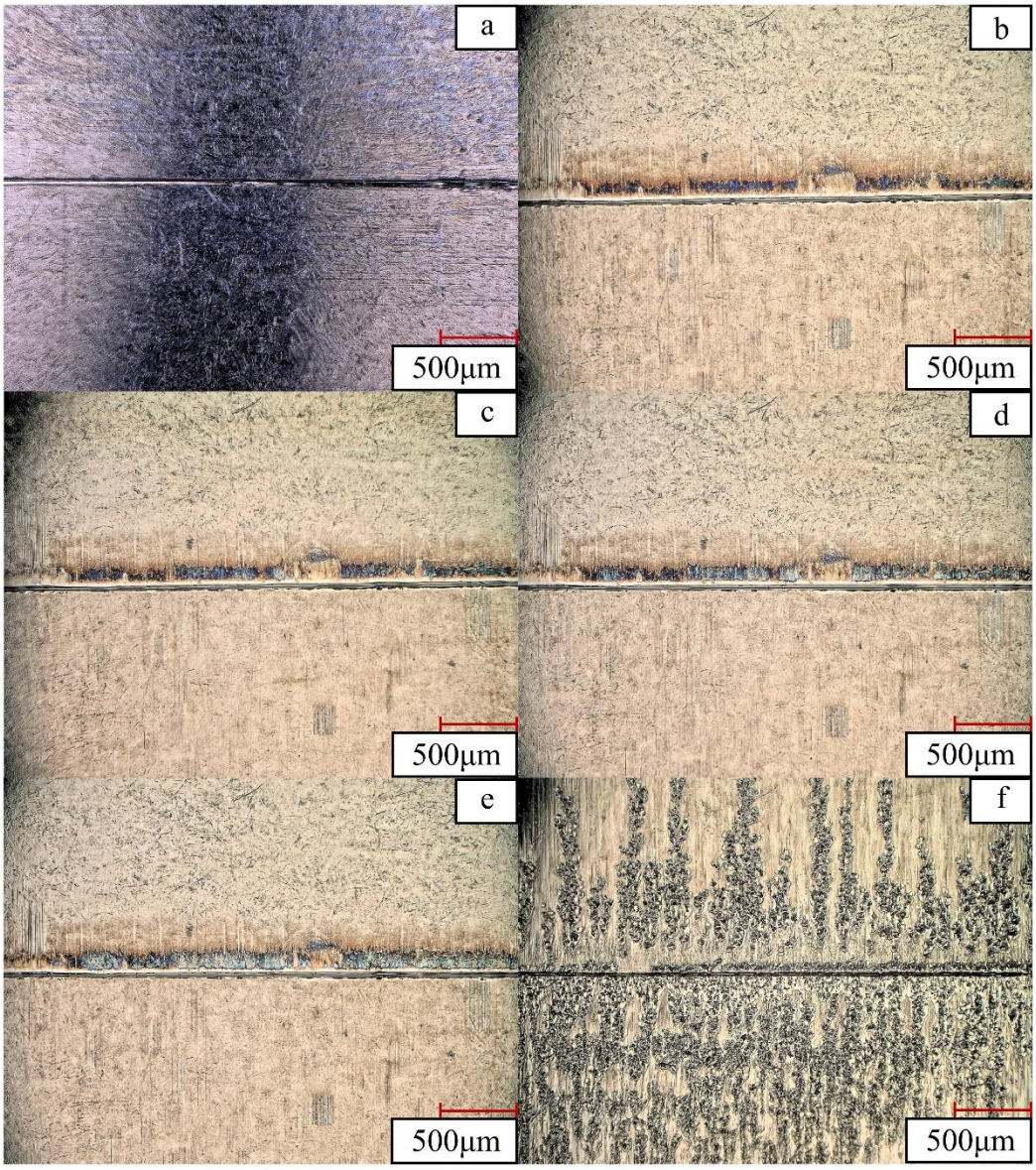

Figure 3.16: 100X microscopic of the HPSTC scratch in site 4 (a) before the test, and after the stages of (b) run-in, (c) A1, (d) A2, (e) A3, and (f) A9.

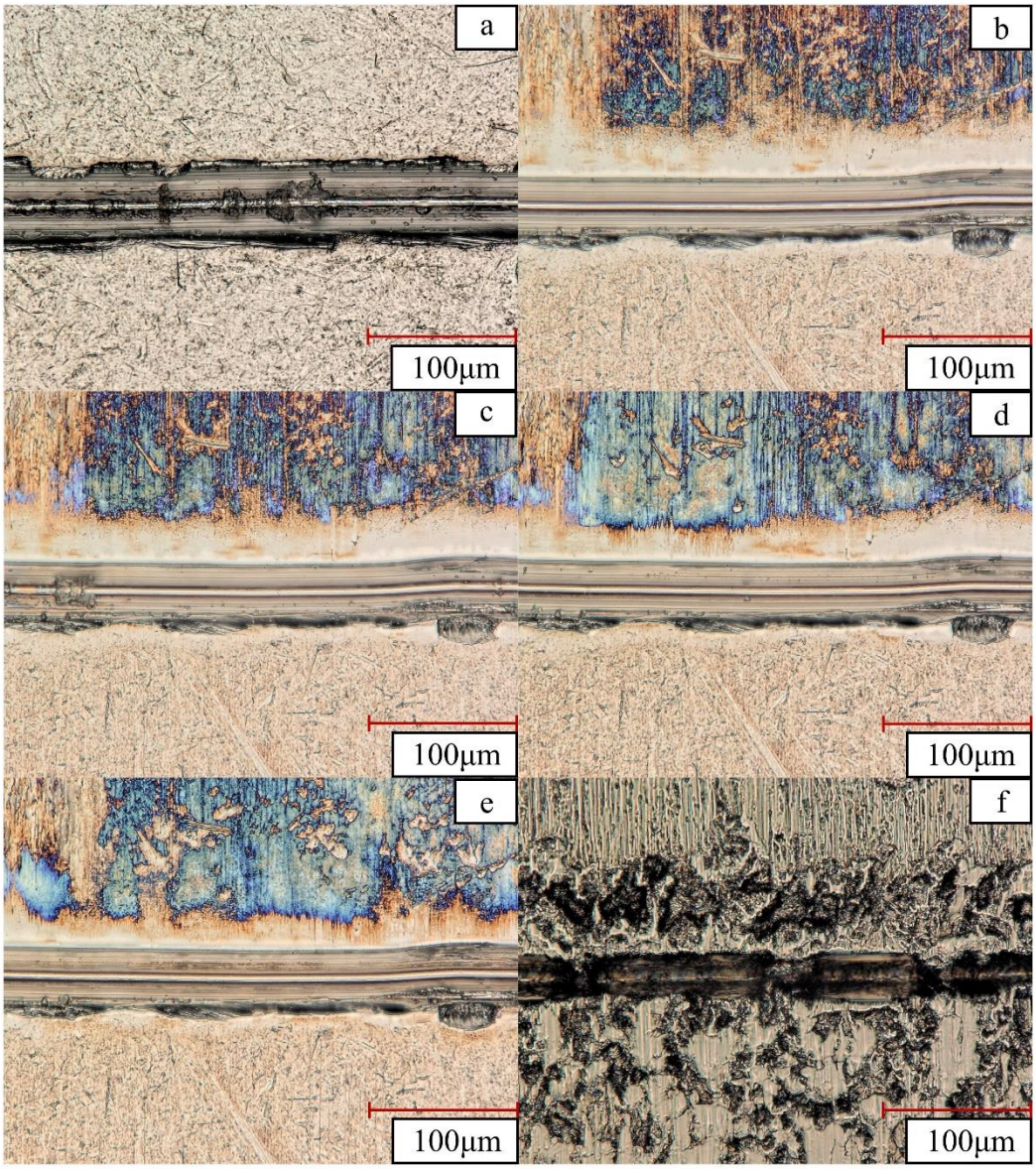

Figure 3.17: 1000X microscopic of the HPSTC scratch in site 4 (a) before the test, and after the stages of (b) run-in, (c) A1, (d) A2, (e) A3, and (f) A9.

to represent the nominal baseline case and three gear pairs whose pinions were scratched intentionally (i) axially along the LPSTC line, (ii) diagonally between the HPSTC and pitch lines, and (iii) axially along the HPSTC line. The baseline gear failed during the last stage of the proposed 15-stage scuffing test protocol. All three types of scratches were observed to severely attenuate gear scuffing performance, as both the LPSTC and diagonal scratches pinion resulted in stage A3 failures, while the HPSTC scratch caused a stage A9 failure.

These results confirm conventional thinking that the highest points of $u_s p$ are near LPSTC and HPSTC, making scratches more critical in those areas. As many elasto-hydrodynamic lubrication parameters are in effect here, it would be premature to make concrete conclusions based on one test per scratch type and size. As such, the data presented in this chapter should be considered as a feasibility study on how surface defects impact the scuffing performance. Also demonstrated is the effectiveness of the proposed experimental methodology in evaluating such effects in a more extensive statistical manner.

Based on the limited data presented, it can be stated that tooth surface scratches have the potential of adversely effecting gear durability. The plus material generated by scratches appears to have no bearing on scuffing failure as it is worn away during run-in and will likely not cause scuffing so long as gears are run-in at low temperatures and slow speeds. However, this material could adhere to and migrate up the tooth face during operation, causing profile-oriented debris damage that could further reduce gear life.

CHAPTER 4

CONCLUSIONS

4.1 Thesis Summary

In this study, otherwise acceptable representative aerospace-grade spur gears were intentionally scratched in a controlled manner to investigate how scratches influence the scuffing performance of gear tooth contacts operating under aerospace conditions. Scratch locations were chosen at regions of the tooth surface that are most susceptible to scuffing failures, near the LPSTC and HPSTC. Two pinions were scratched about the LPSTC and HPSTC, while a third pinion was scratched diagonally between the HPSTC and the pitch point. These three gears, along with an undamaged baseline, were put through a 15-stage scuffing matrix that incrementally increased the torque, speed, and lubricant inlet bulk temperature. The torques, speeds, and lubricant temperatures representative of aerospace operating conditions required the use of specially designed high-speed machines based on the four-square test rig concept.

The resultant scratches were parameterized by their cross-sectional geometries, which were obtained with unfiltered probe-roughness traces. These traces showed that the plus material on the shoulders of the scratch was completely removed during short run-in

stages. Otherwise, scratch geometry remained constant throughout testing. Microscope images revealed surface damage around the scratch for all three of the gears. Bluing and smoothening were observed around the scratches, especially after the scratch in the direction of sliding. This was most prominent on the HPSTC scratch. All three gears failed by scuffing during the lowest temperature tests, much sooner than the undamaged baseline.

4.2 Conclusions

Due to the limited number of damaged gears tested, it was not possible to conclude how scratch size, location, and orientation influence scuffing performance. Rather, this feasibility study should be viewed as a proof-of-concept on how gears with surface defects can be evaluated for their scuffing performance, with fundamental data being provided. As such, the following conclusions that can be drawn from this study are:

- The conventional practice of discarding scratch-damaged gears seems to be warranted, as the surface defects in this study severely attenuated the gears' scuffing performance.
- The positive material displaced during scratching has no direct correlation to scuffing performance because it is almost completely worn away during run-in. However, the brittle failure of plus material during a run-in test could cause debris damage that compromises the surface.
- Besides the plus material, scratch cross-sectional geometry was unchanged throughout testing. As a result, there was no evidence suggesting that surface scratches will heal or wear away during operation.

4.3 Recommendations for Future Work

The proof-of-concept nature of this study requisites more data be collected for any conclusions to be made regarding how surface defects influence the scuffing performance of gear tooth surfaces. As such, the recommendations for future work are as follows:

- Additional scratched gears with the same size, location, and orientation should be run to validate the findings in this study. Scratches at the same locations on the tooth surface, but with decreased depth and width, should be studied to determine how reductions in scratch geometry relate to improvements in scuffing performance. This data could begin to provide insights on what size scratches are tolerable in these zones. Different locations and orientations should also be tested to build up a database from which statistical methods can be used to determine control limits on scratch sizes at different locations based on their orientation.
- Multiple scratches on the tooth surface should be investigated, to determine if defects interact, causing additional heat generation that could cause premature scuffing failures.
- Different types of defects should also be tested, such as dimples, oxidation, or metallic debris adhered to the tooth surface.
- Thermal EHL modeling that includes defects, validated with experiments, could be used to fill the gaps from the inherently limited amount of data that can be collected. Such a model could be used alongside an experimental database to develop control limits for defects on tooth surfaces.

Bibliography

[1] Li, S., "Lubrication and Contact Fatigue Models for Roller and Gear Contacts," Ph.D. Dissertation, The Ohio State University, Columbus, Ohio, 2009.

[2] Liou, J., "A Theoretical and Experimental Investigation of Roller and Gear Scuffing," Ph.D. Dissertation, The Ohio State University, Columbus, Ohio, 2010.

[3] Li, S., Kahraman, A., Anderson, N., and Wedeven, L. D., "A model to predict scuffing failures of a ball-on-disk contact," *Tribology International*, **60**, p. 233–245, 2013.

[4] Handschuh, M. J., Kahraman, A., and Anderson, N. E., "Development of a High-Speed Two-Disc Tribometer for Evaluation of Traction and Scuffing of Lubricated Contacts," *Tribology Transactions*, **63**(3), p. 509–518, 2020.

[5] Handschuh, M. J., Li, S., Kahraman, A., and Talbot, D., "An Experimental – Theoretical Methodology to Develop Scuffing Limits for Relatively Smooth High-Speed Contacts An Experimental – Theoretical Methodology to Develop Scuffing Limits for Relatively Smooth High-Speed Contacts," *Tribology Transactions*, **63**(5), p. 781–795, 2020.

[6] Dowson, D., Higginson, G. R., and Whitaker, A. V., "Elasto-Hydrodynamic Lubrication: A Survey of Isothermal Solutions," *Journal of Mechanical Engineering Science*, **4**(2), p. 121–126, 1962.

[7] Hamrock, B. J., and Dowson, D., "Isothermal Elastohydrodynamic Lubrication of

Point Contacts - 4. Starvation Results.," *American Society of Mechanical Engineers (Paper)*, **99**(1), p. 15–23, 1976.

[8] Hamrock, B. J., and Dowson, D., "Isothermal Elastohydrodynamic Lubrication of Point Contacts - 2. Ellipticity Parameter Results.," *American Society of Mechanical Engineers (Paper)*, **98**(3), p. 375–381, 1975.

[9] Hamrock, B. J., and Dowson, D., "Isothermal Elastohydrodynamic Lubrication of Point Contacts - 3. Fully Flooded Results.," *American Society of Mechanical Engineers (Paper)*, **99**(2), p. 264–275, 1976.

[10] Dowson, D., and Higginson, G. R., "A Numerical Solution to the Elasto-Hydrodynamic Problem," *Journal of Mechanical Engineering Science*, **1**(1), p. 6–15, 1959.

[11] Leque, N., "Development of an Experimental Methodology for Evaluation of Gear Contact Fatigue under High-Power and High-Temperature Conditions Thesis," M.S. Thesis, The Ohio State University, Columbus, Ohio, 2011.

[12] Olson, G., "Experiments on the High-Power and High-Temperature Performance of Gear Contacts," M.S. Thesis, The Ohio State University, Columbus, Ohio, 2012.

[13] Brenneman, J., "An Experimental Study on the Scuffing Performance of High-Power Spur Gears at Elevated Oil Temperatures," M.S. Thesis, The Ohio State University, Columbus, Ohio, 2013.

[14] Krantz, T. L., Alanou, M. P., Evans, H. P., and Snidle, R. W., "Surface Fatigue Lives of Case-Carburized Gears With an Improved Surface Finish," *Journal of Tribology*, **123**(4), p. 709–716, 2001.

[15] Patching, M. J., Kweh, C. C., Evans, H. P., and Snidle, R. W., "Conditions for

scuffing failure of ground and superfinished steel disks at high sliding speeds using a gas turbine engine oil," *Journal of Tribology*, **117**(3), p. 482–489, 1995.

[16] Dempsey, P., and Brandon, E. B., "Validation of Helicopter Gear Condition Indicators Using Seeded Fault Tests," *NASA/TM-2013-217872*, 2013.

[17] Dempsey, P. J., Lewicki, D. G., and Decker, H. J., "Investigation of Gear and Bearing Fatigue Damage Using Debris Particle Distributions," *NASA/TM-2004-212883*, 2004.

[18] Brennan, M., and Reynolds, A., "Use of Vibration Measurements to Detect Local Tooth Defects in Gears – an Experimental Study," *ISVR Technical Report No 267*, 1997.

[19] Lubrecht, A., Dwyer-Joyce, R., and Ioannides, E., "Analysis of the lnfluence of lndentations on Contact Life," *Tribology Series*, **21**, p. 173–181, 1992.

[20] Li, S., and Parmar, U., "The Effects of Microdimple Texture on the Friction and Thermal Behavior of a Point Contact," *Journal of Tribology*, **140**(4), 2018.

[21] Lim, T., "An Experimental Study on the Effects of Debris Damage on Scuffing Performance of Spur Gear Pairs," M.S. Thesis, The Ohio State University, Columbus, Ohio, 2018.

[22] International Organization for Standardization, "Gears - FZG Test Procedures - Part 1: FZG Test Method A/8,3/90 for Relative Scuffing Load-Carrying Capacity of Oils," ISO-14635-1:2000, 2010.

[23] "LDP, Gear Load Distribution Program," Gear and Power Transmission Research Laboratory, The Ohio State University, Columbus, Ohio, 2020.

[24] International Organization for Standardization, "Geometrical Product Specifications

(GPS) — Surface texture: Profile method — Rules and procedures for the assessment of surface texture," ISO-4288:1996, 1996.